IV

ROCK PHYSICS DIAGNOSTIC FOR RESERVOIR CHARACTERIZATION

1. SUMMARY

Rock physics laws that relate porosity, mineralogy (shale content), saturation, and pore-fluid properties to the elastic rock properties -- elastic-wave velocity and impedance -- give the connection between seismic impedance and velocity inversion and physical reservoir properties. They can also be used to produce synthetic seismic images from flow simulation results.

Often, an earth volume under examination has to be described by more that one rock physics law: different depth intervals may have distinctively different velocity-porosity trends due to variations in depositional and diagenetic history. When building a rock physics model, one has to single out various velocity-porosity trends from the entire volume of data and assign these separate trends to appropriate depth intervals and depositional sequences. This procedure is called **rock physics diagnostic**. Rock physics diagnostic is typically conducted on well log and core data.

Rock physics diagnostic allows not only to produce useful relations between seismic observables and porosity. It allows one to describe the texture of rock: the position of diagenetic cement; grain size sorting; effect of clay, etc.

This texture description in turn can be linked to the depositional and stratigraphic features of the subsurface.

For example, well-sorted grains with small amount of intergranular cement may correspond to a high-energy stream whereas deteriorating sorting is likely to be found in a low-energy depositional environment downstream. Sorting and cementation in turn determine permeability and strength.

2. INTRODUCTION

Rock physics laws that relate porosity, mineralogy (shale content), saturation, and pore-fluid properties to the elastic rock properties -- elastic-wave velocity and impedance -- give the connection between flow simulation and synthetic seismic imaging.

These laws can be obtained from:

(a) core measurements where velocity, mineralogy, density, and porosity are measured simultaneously on a suite of rock samples representative of the earth volume subject to modeling; and

(b) well log data that include velocity, mineralogy (gamma-ray), saturation, density, and porosity curves.

Often, an earth volume under examination has to be described by more that one rock physics law: different depth intervals may have distinctively different velocity-porosity trends due to variations in depositional and diagenetic history. When building a rock physics model,

one has to single out various velocity-porosity trends from the entire volume of data and assign these separate trends to appropriate depth intervals and depositional sequences. This procedure is called ***rock physics diagnostic***.

The work space for rock physics diagnostic is the **rock physics plane** that may be

(a) velocity-porosity;

(b) impedance-porosity; and/or

(c) modulus-porosity plane.

The P- (Ip) and S-impedance (Is) are defined, respectively, as

$$I_p = V_p \rho_b, \quad I_s = V_s \rho_b,$$

where V_p and V_s are the P- and S-wave velocity, respectively; and ρ_b is the bulk density.

The compressional (M) and shear (m) moduli are defined, respectively, as

$$M = V_p^2 \rho_b, \quad \mu = V_s^2 \rho_b.$$

Below, we show how log data measured in a continuous depth interval (Figure 1) can separate into three distinctively different trends (Figure 2).

It also follows from Figure 2 that the rock physics trends appear to be "sharper" in the impedance-porosity or modulus-porosity plane than they are in the velocity-porosity plane. This is why we recommend using impedance or elastic modulus instead of velocity when diagnosing rock.

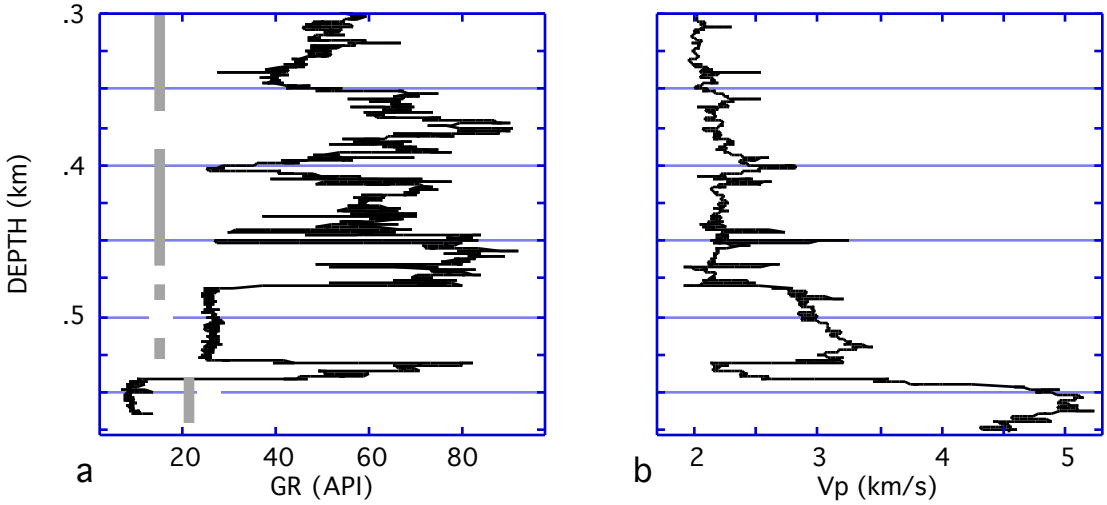

Figure 1. Well log data versus depth (fictitious). a. Gamma-ray; b. velocity.

During rock diagnostic, it is important to eliminate from consideration as many factors affecting velocity as possible. One of such factors, that can be easily eliminated, is saturation. Velocity may strongly depend on saturation and/or pore fluid compressibility that, in turn, may

vary with depth. Because of varying saturation or fluid properties, the same rock type may appear to have no velocity-porosity trend at all (Figure 3). In fact, identical samples of rock (especially soft rock) will have very different velocity, impedance, and moduli, if saturated with different fluids.

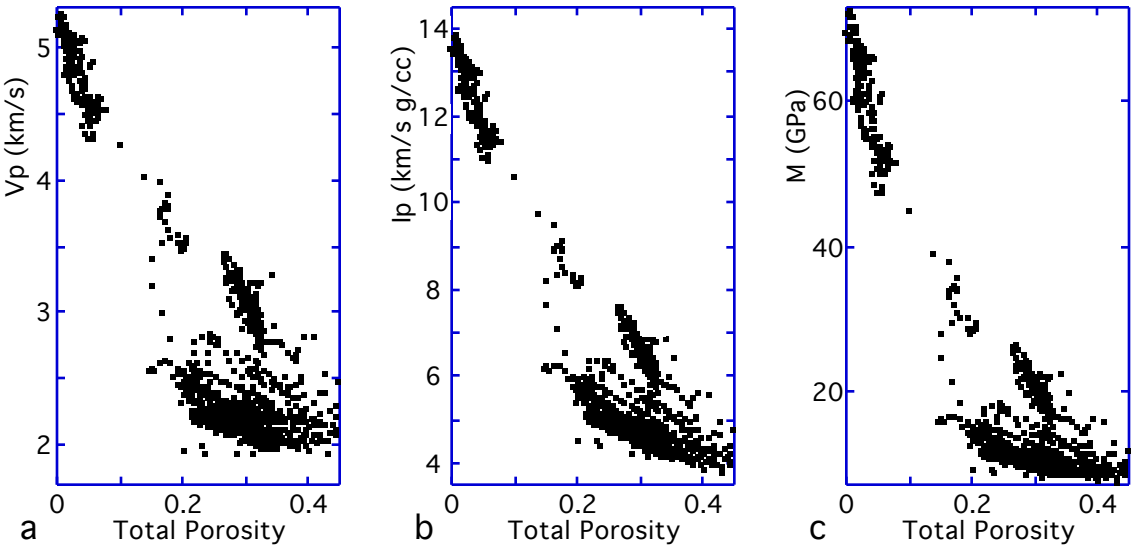

Figure 2. Cross-plotting well-log data in the rock physics plane. a. Velocity versus porosity; b. impedance versus porosity; c. modulus versus porosity. The trends marked correspond to the depth intervals shown in Figure 1a.

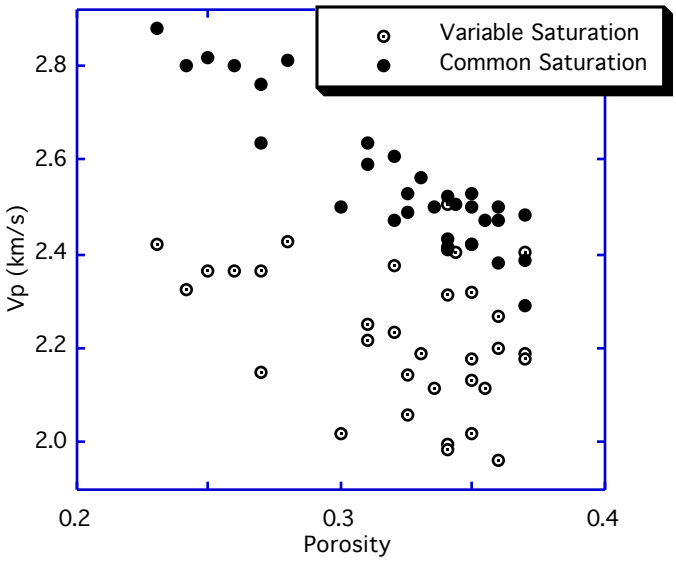

Figure 3. Velocity versus porosity for a soft rock dataset, with variable and common saturation.

To eliminate this additional complication, one has to bring the entire interval to ***common pore fluid saturation***. This common saturation process consists of three steps:

Step 1: Use well log data to calculate the elastic moduli of the dry rock.

Step 2: Use the dry-rock elastic moduli thus obtained to calculate those of rock saturated with the same fluid for the entire interval or data set.

Step 3: Use the common-fluid rock moduli to calculate velocity and impedance as needed.

The details of fluid substitution needed for these tasks are given above. When using core velocity data, dry-rock measurements are preferred.

3. Three Types of Rock Physics Diagnostic

We define rock physics diagnostic as the procedure of establishing elastic moduli versus porosity relations for the volume of earth under examination. The principal data source for rock physics diagnostic are well logs and/or core measurements.

Once the moduli-porosity relations are established, it is easy to transform them into impedance-porosity and velocity-porosity relations.

The two types of rock physics diagnostic are:

Type 1: Finding a theoretical modulus-porosity relation that describes the dataset.

Type 2: Finding a data set that is elastically analogous to the dataset under investigation.

Type 3: Finding an empirical fit from the data.

It is understood in the second case that the analog has been well studied and some of its properties (e.g., a relation between Vp and Vs) can be used for the data set under investigation. The three types of rock physics diagnostic can be used separately or simultaneously since they complement each other.

DIAGNOSTIC 1: THEORETICAL MODULUS-POROSITY RELATIONS

This procedure consists of the following steps:

STEP 1: Bring the entire interval under examination, or the suite of core data, to common pore fluid saturation. Calculate the elastic moduli at this common saturation. This step includes the following sub-steps:

Substep 1.1: Calculate the effective bulk moduli of pore fluid components in the interval. Based on these, calculate the effective bulk modulus $\overline{K}_{fluid}$ of the pore fluid mixture as

$$\frac{1}{\overline{K}_{fluid}} = \frac{S_{gas}}{K_{gas}} + \frac{S_{oil}}{K_{oil}} + \frac{S_{br}}{K_{br}},$$

where $S_{gas,oil,br}$ and $K_{gas,oil,br}$ are the saturations and bulk moduli of the gas, oil, and brine, respectively.

Substep 1.2: Calculate the rock bulk modulus K_{log} from the well log (or core) data as

$$K_{log} = \rho_b (V_p^{\,2} - 4V_s^{\,2}/3).$$

If the shear-velocity data are not available, calculate the compressional modulus M_{log} as

$$M_{log} = \rho_b V_p^{\,2}.$$

Tips to Substep 1.2.

1. Even if the shear-wave data are available, calculate the compressional modulus anyway since the shear-wave data may be of low quality.

Substep 1.3: Calculate the dry-rock bulk modulus from the rock bulk modulus as

$$K_{dry} = K_{mineral}\frac{1-(1-\phi)K_{log}/K_{mineral}-\phi K_{log}/\overline{K}_{fluid}}{1+\phi-\phi K_{mineral}/\overline{K}_{fluid}-K_{log}/K_{mineral}},$$

where ϕ is total porosity, and $K_{mineral}$ is the bulk modulus of the mineral phase (for calculating $K_{mineral}$.

If the shear-velocity data are not available, calculate the dry-rock compressional modulus M_{dry} as

$$M_{dry} = M_{mineral}\frac{1-(1-\phi)M_{log}/M_{mineral}-\phi M_{log}/\overline{K}_{fluid}}{1+\phi-\phi M_{mineral}/\overline{K}_{fluid}-M_{log}/K_{mineral}},$$

where $M_{mineral} = K_{mineral} + 4\mu_{mineral}/3$, and $\mu_{mineral}$ is the shear modulus of the mineral phase (for calculating $\mu_{mineral}$.

Tips to Substep 1.3.

1. Even if the shear-wave data are available, calculate the dry-rock compressional modulus anyway since the shear-wave data may be of low quality.

2. Do not be discouraged if the elastic moduli of the dry rock have unreasonable (e.g., negative) values for some data points. This may be due to small errors in input parameters (porosity, mineral's elastic moduli, etc.). These errors will be corrected in Substep 1.4 below.

Substep 1.4: Calculate the bulk modulus K_{common} of the rock saturated with common (uniform for the entire interval or data set) pore fluid:

$$K_{common} = K_{mineral}\frac{\phi K_{dry}-(1+\phi)K_{cf}K_{dry}/K_{mineral}+K_{cf}}{(1-\phi)K_{cf}+\phi K_{mineral}-K_{cf}K_{dry}/K_{mineral}},$$

where K_{cf} is the bulk modulus of the common fluid. As common fluid use the stiffest pore-fluid component (formation water or mud filtrate).

We emphasize that K_{cf} has to be the same for the entire interval or data set.

Next, calculate the compressional modulus M_{common} of the rock saturated with common (uniform for the entire interval or data set) pore fluid:

$$M_{common} = K_{common} + \rho_b 4V_s^{\,2}/3.$$

If the shear-velocity data are not available, calculate the compressional modulus M_{common} of the rock saturated with common pore fluid as

$$M_{common} = M_{mineral} \frac{\phi M_{dry} - (1+\phi) K_{cf} M_{dry} / M_{mineral} + K_{cf}}{(1-\phi) K_{cf} + \phi M_{mineral} - K_{cf} M_{dry} / M_{mineral}}.$$

Tips to Substep 1.4.

1. Even if the shear-wave data are available, use the last equation to calculate the compressional modulus of the rock saturated with common pore fluid anyway since the shear-wave data may be of low quality. Compare it to the modulus obtained from the previous equation for quality control.

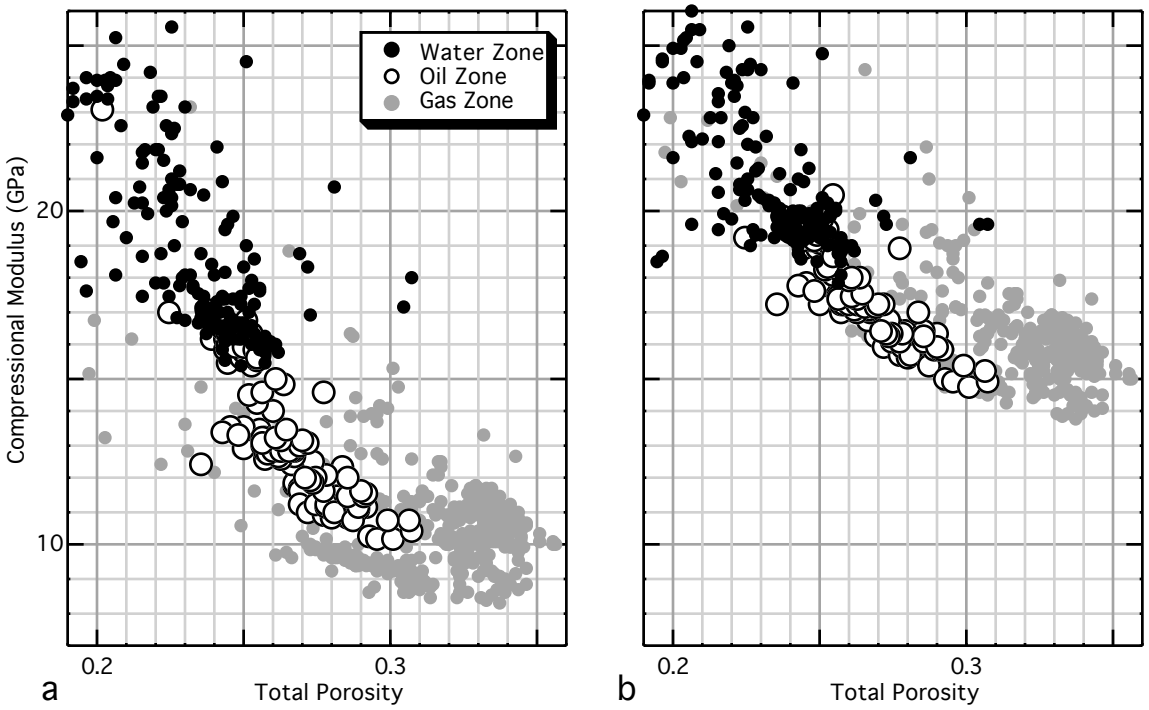

Figure 4. Example of bringing an interval to a common saturation. a. Compressional modulus directly from log data plotted versus porosity. Trends seem to be different for water, oil, and gas zones. b. Data at common saturation (formation water). Most of the data exhibit a single trend.

STEP 2: Cross-plot the compressional modulus at common saturation versus porosity and fit appropriate theoretical modulus-porosity models.

Substep 2.1: Plot the compressional modulus versus porosity for the entire interval or data set or for selected parts of it. Use plotting package where you can easily superimpose theoretical model curves or other datasets. Some candidates are Excel, KaleidaGraph, Matlab. An example in Figure 2.5 shows how the well-log data from an interval where a very clean (low gamma ray) interval is present, separates into two parts when the compressional modulus is plotted versus total porosity. The upper branch of the data is form the low-GR interval whereas the lower branch is from the rest of the interval where shale is present.

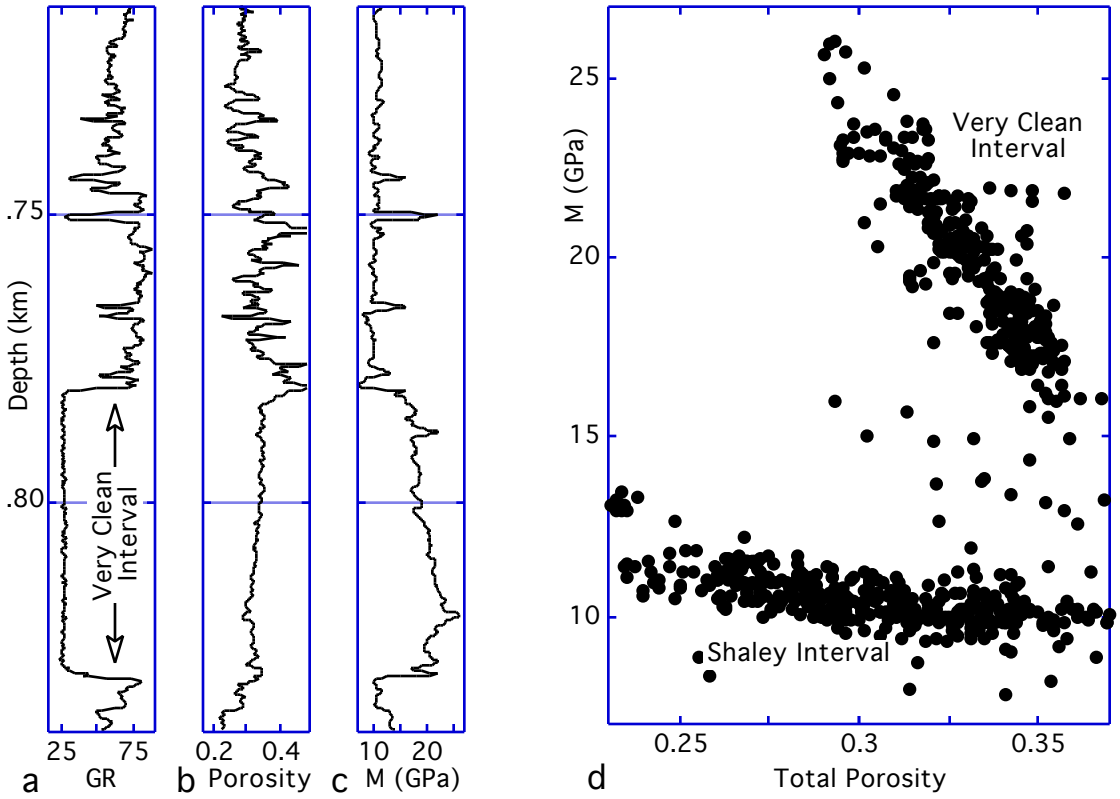

Figure 5. Example of cross-plotting compressional modulus versus porosity. a. Gamma-ray versus depth in the interval under investigation. b. Total porosity versus depth. c. Compressional modulus at common saturation versus depth. d. Compressional modulus at common saturation versus porosity.

Substep 2.2: Select the appropriate rock physics theory (theories) and superimpose on the modulus-porosity cross-plot. When using a theoretical relation, make sure that the pore fluid is the same as the common pore fluid used in Step 1. It is not easy to select the appropriate theory. Below, we give equations for existing theoretical and empirical modulus-porosity equations and recommend applying them depending on porosity range and rock type. The more models the user superimposes on the modulus-porosity cross-plot the better is the chance of finding the appropriate theory.

Example: Consider the log data in Figure 5. The rock is high-porosity sandstone. Appropriate theories to try are: (a) cementation theory; and (b) unconsolidated rock theory. Both provide the dry-rock elastic moduli. We use Gassmann's equation to theoretically saturate these dry rocks with the common pore fluid. The results are shown in Figure 6a. We can see that the unconsolidated rock theory describes the part of the interval where shale is present, and the cementation theory approximately describes the clean (low-GR) interval.

Substep 2.3: Adjust the theory selected. Practically every rock physics modulus-porosity model has adjustable parameters. They may mineral elastic moduli, critical porosity, etc. (see

below in model description). As we see in Figure 6a, the Model A curve computed with default input parameters does not fit the data precisely.

Our next attempt is to refine the fit between the theory and the data by adjusting some input parameters (of course, within reasonable ranges).

This procedure is illustrated in Figure 6b where we changed the critical porosity value from 0.38 in the default mode to 0.36 to fit the data.

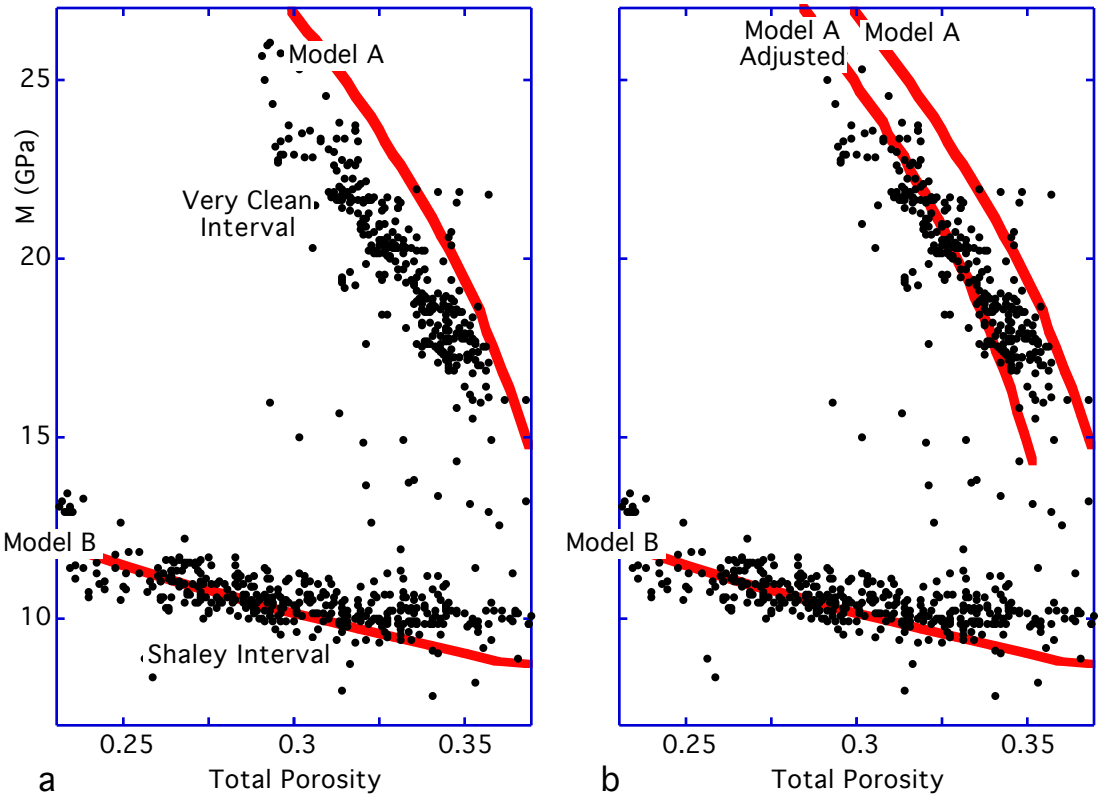

Figure 6. a. Selecting the appropriate rock physics models. b. Adjusting the models. Model A is from cementation theory; Model B is from unconsolidated rock theory.

As a result of Step 2, we will have modulus-porosity models that describe the data set under examination on the interval basis. Now these models are ready to be applied to the entire volume of rock.

As we move in space, porosity and saturation may change, but the models (we assume) will remain the same. It is very important to know (or assume) the spatial extension of the intervals to which specific models have been fitted.

For example, in the above-discussed case, one has to know the spatial configuration of clean cemented rocks that give very low gamma-ray signature (Figure 5).

ROCK PHYSICS DIAGNOSTIC FLOWCHART

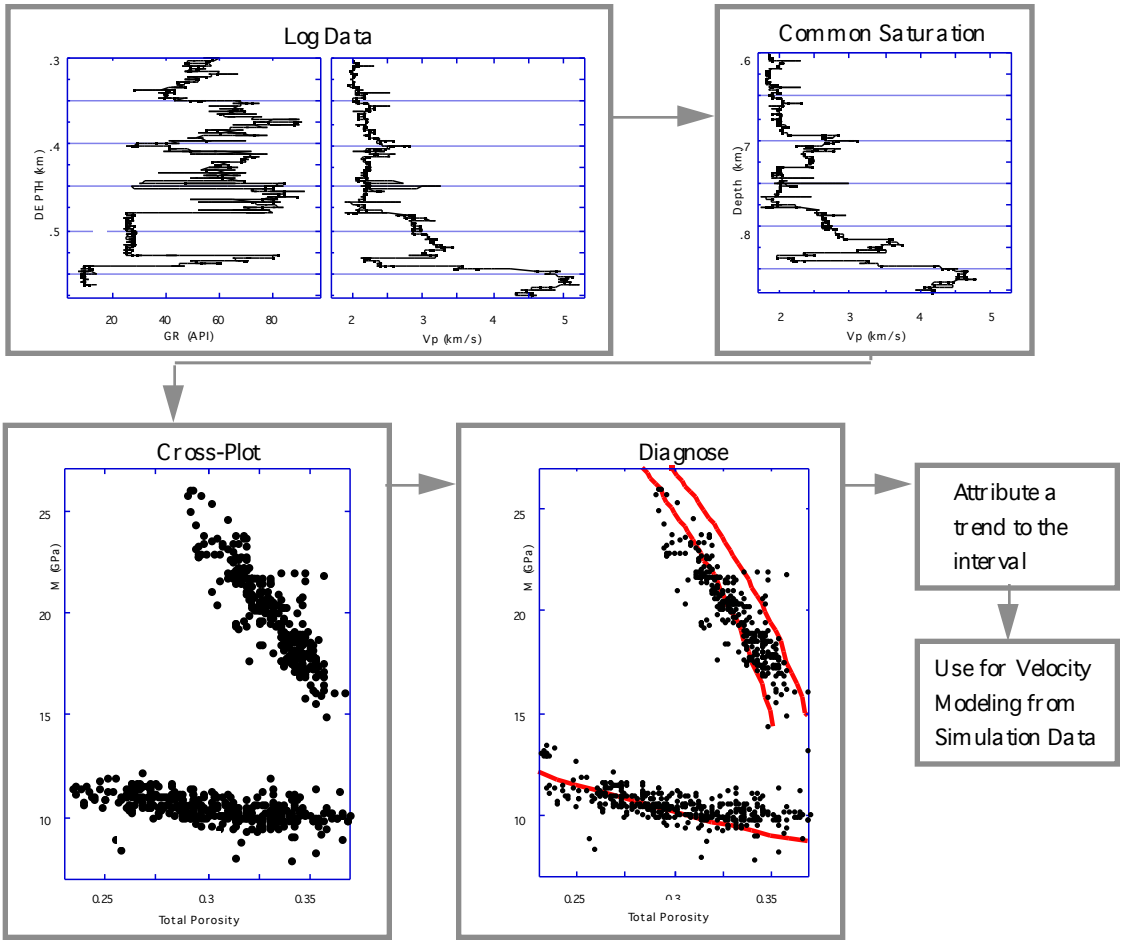

SUPPLEMENT TO DIAGNOSTIC 1: GUIDE TO MODULUS-POROSITY MODELS

For detailed assumptions, limitations and applicability of the models see Mavko, Mukerji, and Dvorkin, 1998, "The Rock Physics Handbook." Below, velocity is in km/s; porosity is in volumetric fraction (pu); clay content is in volumetric fraction; density is in g/cm^3; and modulus is in GPa.

1. Wyllie et al. (1956) Time Average (Empirical)

$$\frac{1}{V_p} = \frac{\phi}{V_{p-fl}} + \frac{1-\phi}{V_{p-mineral}},$$

where ϕ is total porosity; and V_{p-fl} and $V_{p-mineral}$ are the compressional-wave velocity in the common pore fluid and mineral phase, respectively. V_{p-fl} should be calculated from the bulk modulus $\overline{K}_{fluid}$ and fluid density $\overline{\rho}_{fluid}$ as

$$V_{p-fl} = \sqrt{\overline{K}_{fluid} / \overline{\rho}_{fluid}}.$$

$V_{p-mineral}$ should be calculated from $K_{mineral}$, $\mu_{mineral}$, and mineral density $\rho_{mineral}$ as

$$V_{p-mineral} = \sqrt{(K_{mineral} + 4\mu_{mineral}/3)/\rho_{mineral}}.$$

To calculate the compressional modulus from Wyllie's equation, use $M_{common}^{Wyllie} = \rho_b V_p^2$, where ρ_b is bulk density of the rock saturated with common fluid.

Adjustable parameters in Wyllie's equation are the elastic moduli of the mineral components that make up the mineral phase. For example, for quartz, the bulk modulus may be chosen between 34 GPa and 38 GPa; for clay these moduli may span quite a wide interval (see Mavko et al., 1998). Wyllie et al. recommend the following ranges for $V_{p-mineral}$:

Rock Type	Mineral Velocity (km/s)
Sandstone	5.480 to 5.950
Limestone	6.400 to 7.000
Dolomite	7.000 to 7.925

This model has a very simple analytical expression but is strictly empirical. It can be applied only to fully-saturated rocks and should not be applied to soft unconsolidated rocks.

2. Raymer-Hunt-Gardner (1980) Relations (Empirical)

$$V_p = (1-\phi)^2 V_{p-mineral} + \phi V_{p-fl} \quad \text{for} \quad \phi < 37\%;$$
$$M_{common}^{Raymer} = \phi / \bar{K}_{fluid} + (1-\phi)/(K_{mineral} + 4\mu_{mineral}/3) \quad \text{for} \quad \phi > 47\%;$$
$$1/V_p = 10[(0.47-\phi)/V_{37} + (\phi - 0.37)/V_{47}].$$

where V_{37} and V_{47} are calculated from the first-line equation at $\phi = .37$ and second-line equation at $\phi = .47$, respectively. As in the Wyllie model, the compressional modulus at common saturation is $M_{common}^{Raymer} = \rho_b V_p^2$. This model is strictly empirical and mimics real data much better than Wyllie's model does. It should not be applied to soft unconsolidated rocks.

3. Han's (1986) Relations (Empirical)

Clean Water-Saturated Sandstones Effective Pressure 40 MPa:

$$V_p = 6.08 - 8.06\phi, \quad V_s = 4.06 - 6.28\phi.$$

Shaley Water-Saturated Sandstones
Effective Pressure:

40 MPa: $V_p = 5.59 - 6.93\phi - 2.18C, \quad V_s = 3.52 - 4.91\phi - 1.89C;$

30 MPa: $V_p = 5.55 - 6.96\phi - 2.18C, \quad V_s = 3.47 - 4.84\phi - 1.87C;$

20 MPa: $V_p = 5.49 - 6.94\phi - 2.17C, \quad V_s = 3.39 - 4.73\phi - 1.81C;$

10 MPa: $V_p = 5.39 - 7.08\phi - 2.13C, \quad V_s = 3.29 - 4.73\phi - 1.74C;$

5 MPa: $V_p = 5.26 - 7.08\phi - 2.02C, \quad V_s = 3.16 - 4.77\phi - 1.64C.$

Shaley Room-Dry Sandstones Effective Pressure 40 MPa:

$$V_p = 5.41 - 6.35\phi - 2.87C, \quad V_s = 3.57 - 4.57\phi - 1.83C.$$

In Han's equations, C is the volumetric clay content in rock. These equations have been obtained from laboratory ultrasonic measurements on sandstones saturated with pure water. They cannot be adjusted for any other pore fluid. Therefore, when using them to diagnose rock, use pure water (density 1 g/cm^3 and bulk modulus 2.25 GPa) as common fluid. Be cautious when using these equation at small (below 30 MPa) effective pressure. The ultrasonic velocity dispersion effect may bias the results. The compressional modulus can be calculated from velocity and bulk density as $M_{common}^{Han} = \rho_b V_p^{\,2}$.

4. Tosaya and Nur (1982) Relations (Empirical)

Shaley Water-Saturated Sandstones Effective Pressure 40 MPa:

$$V_p = 5.8 - 8.6\phi - 2.4C, \quad V_s = 3.7 - 6.3\phi - 2.1C,$$

In these equations, C is the volumetric clay content in rock. These equations have been obtained from laboratory ultrasonic measurements on high-shale-content sandstones saturated with pure water. They cannot be adjusted for any other pore fluid. Therefore, when using them to diagnose rock, use pure water (density 1 g/cm^3 and bulk modulus 2.25 GPa) as common fluid. See velocity dispersion effect warning for Han's equations. The compressional modulus is $M_{common}^{Tosaya} = \rho_b V_p^{\,2}$.

5. Eberhart-Phillips (1989) Relations (Empirical)

Shaley Water-Saturated Sandstones

$$V_p = 5.77 - 6.94\phi - 1.73\sqrt{C} + 0.446(P - e^{-16.7P}),$$
$$V_s = 3.70 - 4.94\phi - 1.57\sqrt{C} + 0.361(P - e^{-16.7P}).$$

This equations are very approximate and should be used for rough estimates only. In these equations, C is the volumetric clay content in rock and P is the effective pressure (overburden minus pore pressure) in kilobars. These equations have been obtained from laboratory ultrasonic measurements on high-shale-content sandstones saturated with pure water. They cannot be adjusted for any other pore fluid. Therefore, when using them to diagnose rock, use pure water (density 1 g/cm^3 and bulk modulus 2.25 GPa) as common fluid. See velocity dispersion effect warning for Han's equations below. The compressional modulus is $M_{common}^{Tosaya} = \rho_b V_p^{\,2}$.

6. Critical Porosity (Nur et al., 1998) -- Modified Voigt Average (heuristic)

$$K_{dry} = K_{mineral}(1 - \phi / \phi_c), \mu_{dry} = \mu_{mineral}(1 - \phi / \phi_c),$$

where ϕ_c is the critical porosity. See details in Mavko et al., 1998. To calculate the saturated-rock moduli, use Gassmann's fluid substitution equation. Below is a table for critical porosity

values in different rocks. This model tends to over-estimate the elastic moduli. Adjustable parameters in the Critical Porosity model are: critical porosity, and the bulk and shear moduli of the mineral phase.

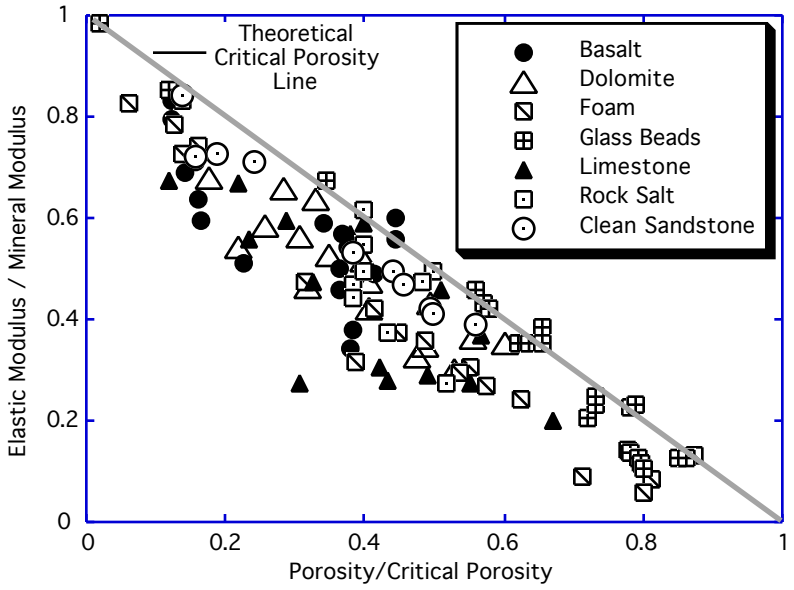

Figure 7. Critical porosity model.

12. Model for Chalks of Walls et al., 1998 (Theoretical):

The theoretical curve in the modulus-porosity plane connects a high-porosity datapoint that has to be manually picked from the data to the zero-porosity point at which the moduli of the rock are those of the mineral phase. The connecting curve is the upper Hashin-Shtrikman bound with the stiffest component being the mineral and the softest one having the elastic moduli of the selected high-porosity point. The high-porosity initial point has to be selected based on the dry-frame moduli.

Inputs: initial (high) porosity chosen from the data, in fraction (ϕ_0);

bulk modulus at ϕ_0 in GPa (K_0);

shear modulus at ϕ_0 in GPa (G_0);

bulk modulus of the solid phase in GPa ($K_{mineral}$);

shear modulus of the solid phase in GPa ($G_{mineral}$);

total porosity ϕ (varies between ϕ_0 and zero).

The effective bulk (K_{dry}) and shear (G_{dry}) moduli of dry rock are:

$$K_{dry} = \left[\frac{\phi/\phi_0}{K_0 + \frac{4}{3}G_{mineral}} + \frac{1-\phi/\phi_0}{K_{mineral} + \frac{4}{3}G_{mineral}}\right]^{-1} - \frac{4}{3}G_{mineral},$$

$$G_{dry} = \left[\frac{\phi/\phi_0}{G_0 + z} + \frac{1-\phi/\phi_0}{G_{mineral} + z}\right]^{-1} - z, \quad z = \frac{G_{mineral}}{6}\frac{9K_{mineral} + 8G_{mineral}}{K_{mineral} + 2G_{mineral}}.$$

Adjustable parameters are: ϕ_0; K_0; G_0; $K_{mineral}$; and $G_{mineral}$. Example is given below for Ekofisk field where porosity had to be tracked seismically to track production fronts.

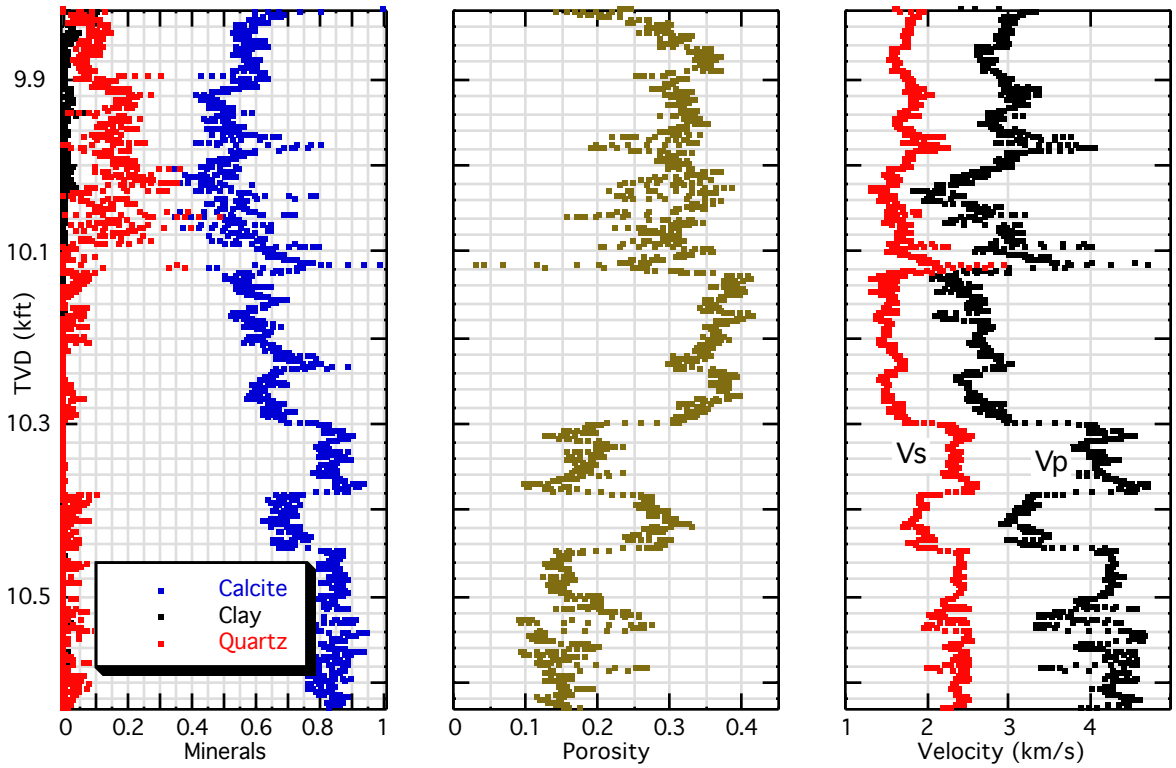

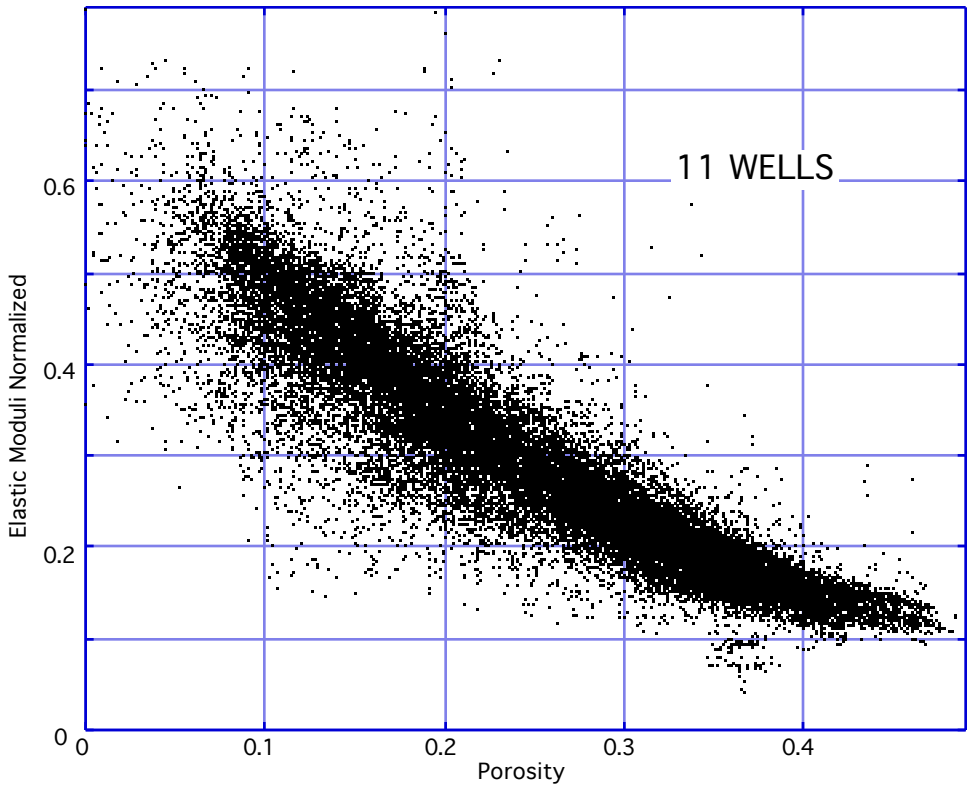

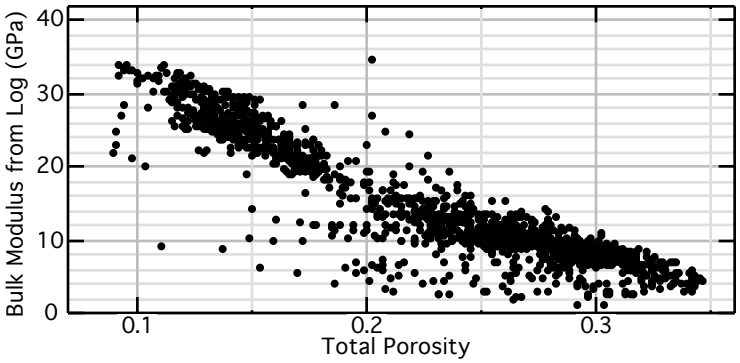

Figure 8. Example of chalk data. Bulk modulus (taken directly from log data) versus porosity.

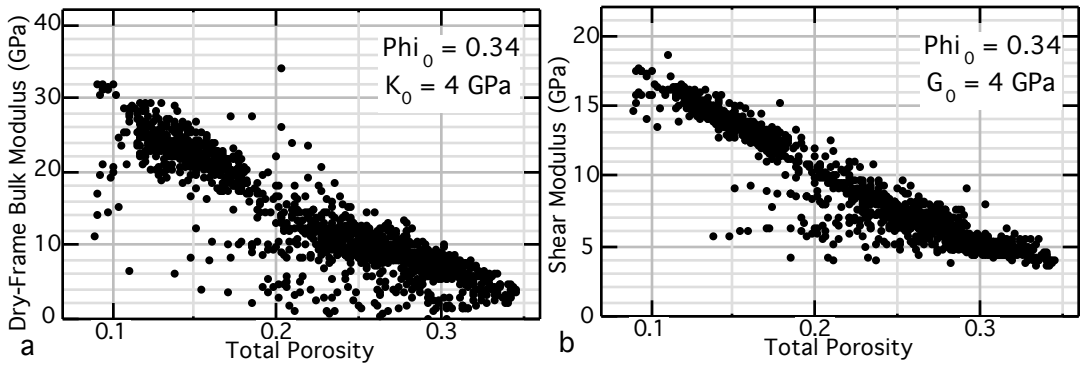

Figure 9. Dry-frame bulk modulus (a) and shear modulus (b). The initial (high) porosity and the corresponding moduli are picked from the plots.

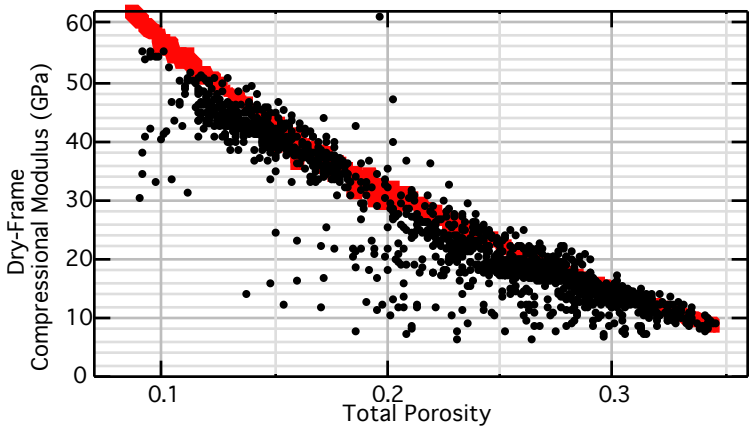

Figure 10. Dry-frame compressional modulus matched by the model curve.

DIAGNOSTIC 2: FINDING ANALOGOUS DATA SET

This procedure consists of the following steps:

STEP 1: Bring the entire interval under examination, or the suite of core data, to common pore fluid saturation and calculate the elastic moduli. This step is the same as in DIAGNOSTIC 1.

STEP 2: Cross-plot the compressional modulus at common saturation versus porosity and add on top of this cross-plot well-understood data that may be elastically close to the data set to be diagnosed. The moduli of the analogous data set should be recalculated to have the same common fluid as the data set under examination. This data set should be taken at the same effective pressure as the data set under examination. This step requires calibration datasets.

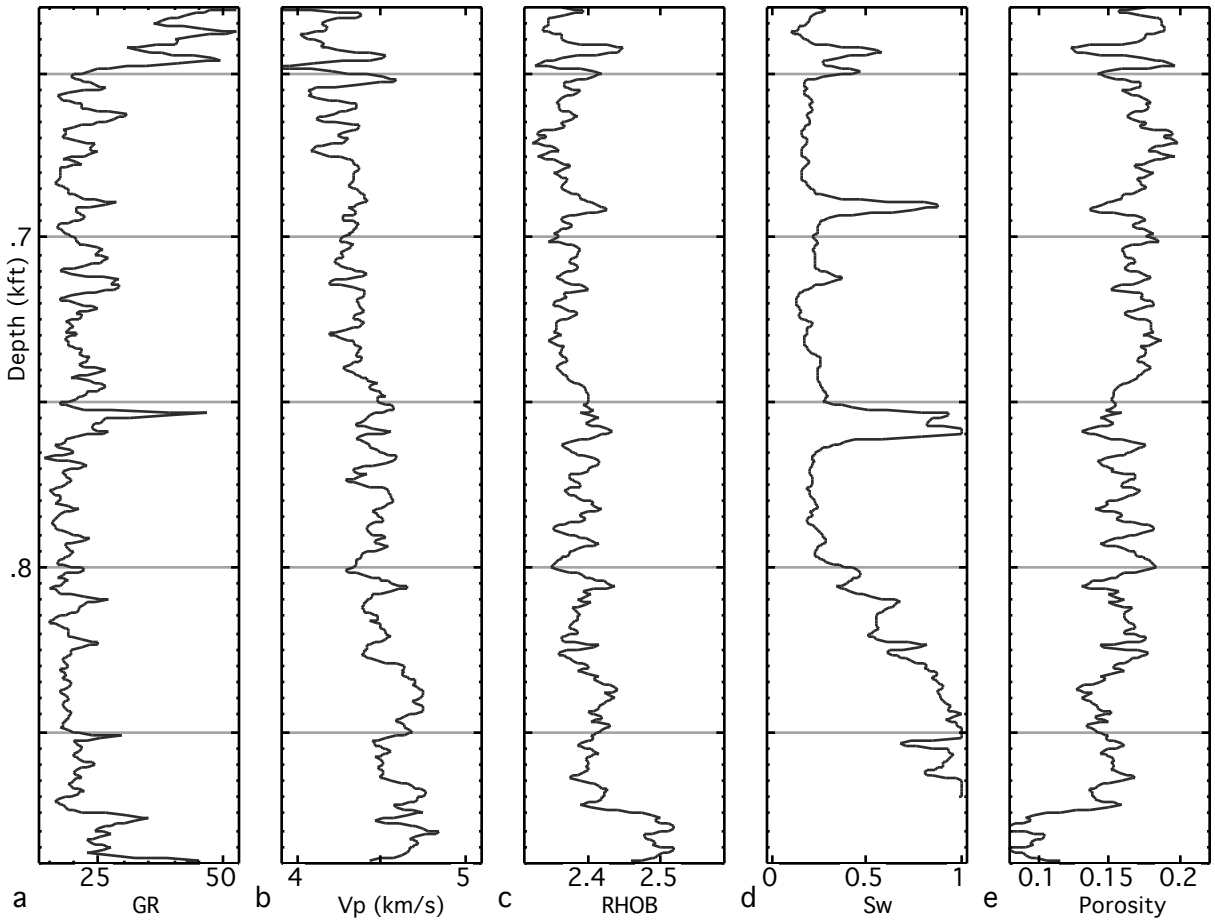

Figure 11. Log curves versus depth: gamma ray; velocity; density; saturation; and porosity.

In Figure 11 we show a set of well log measurements in a vertical well drilled through deep consolidated sandstones. Figure 11a (GR versus depth) indicates that these sandstones are very clean, especially in the lower part of the interval, with only a few thin shaley layers. Only compressional-wave measurements are available. The goal is to diagnose these rocks and establish velocity-porosity relations for both P- and S-waves. We choose the common saturation fluid as a mixture of oil and formation water and cross-plot (Figure 12) P-impedance versus density-porosity (total porosity calculated from the bulk density data). In Figure 12a we plot the data from the entire interval under examination. These data show a fairly tight impedance-porosity trend that can be used for further modeling. Even better trend appears if

we plot only the cleanest sandstone data points versus porosity (Figure 12b). In Figure 13, we replot the same data as in Figure 12 with laboratory data set plotted on top. These superimposed data points are from Han's (1986) data set.

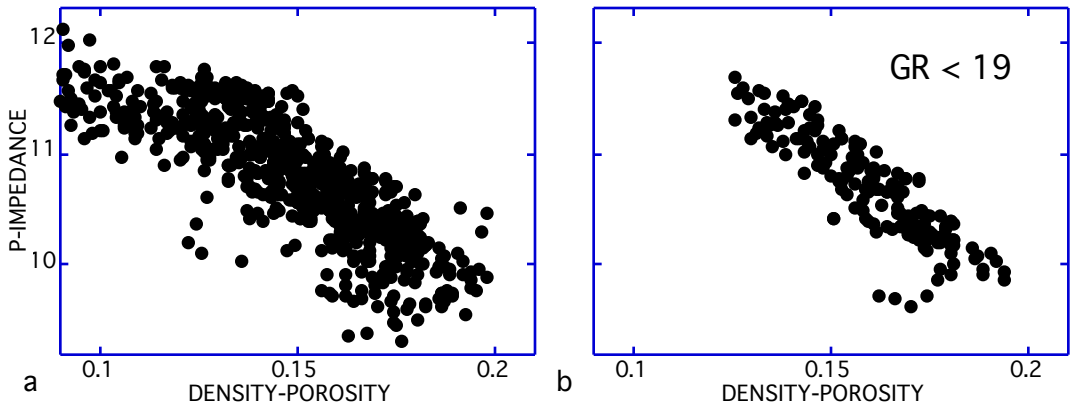

Figure 12. P-impedance versus porosity. a. For the entire interval. b. For the cleanest parts where gamma-ray count is below 19 API.

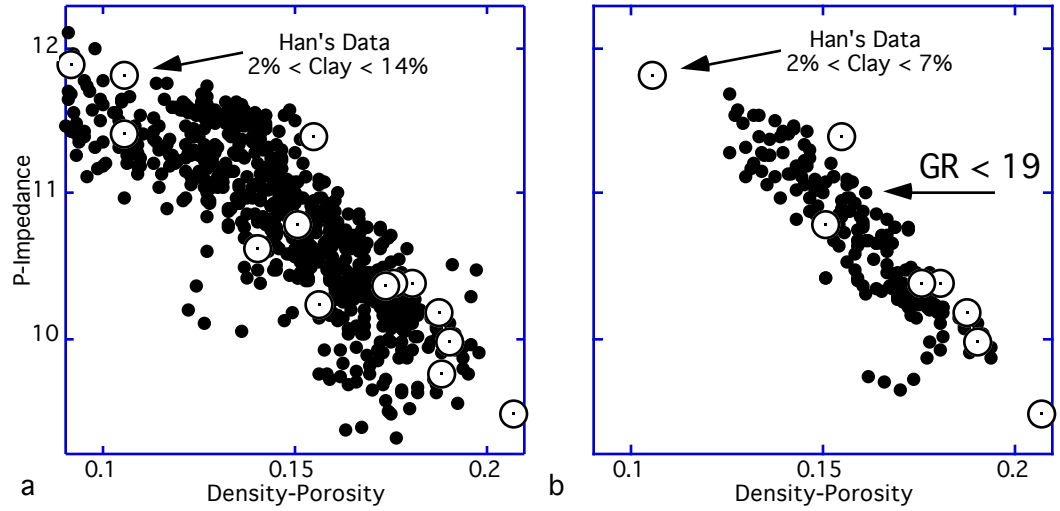

Figure 13. P-impedance versus porosity. a. Entire interval. b. Cleanest parts where gamma-ray count is below 19 API. Superimposed are data points from Han's (1986) dataset. a. Clay content between 2% and 14%. b. Clay content between 2% and 7%.

We can see now that for the entire interval trend (Figure 13a) can be approximated by that of a subset of Han's data set where the volumetric clay content is between 2% and 14%. The cleanest-sand trend (Figure 13b) can be approximated by that of a subset of Han's data set where the volumetric clay content in the rock is between 2% and 7%. Based on this similarity between the well log data under examination and Han's data, we speculate that all rock physics relations valid for the selected Han's data points hold for the well log data. The desired Vs versus Vp relations are plotted below in Figure 14. They can be used for the well log data under examination.

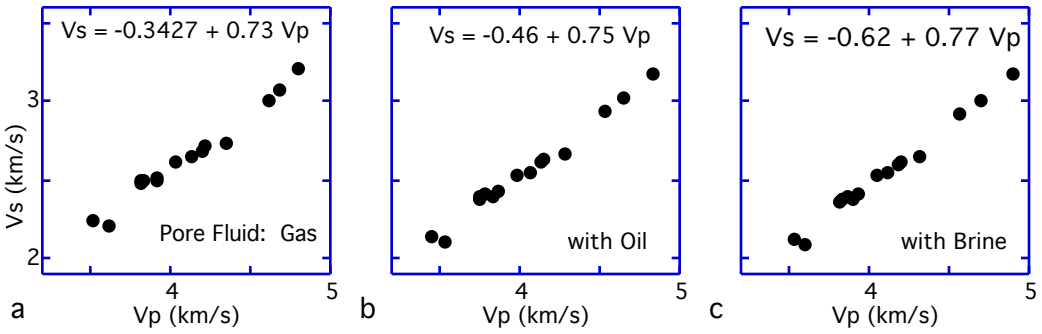

Figure 14. Vp versus Vs for Han's dataset for (a) gas-saturated rocks; (b) oil-saturated rocks; and (c) brine-saturated rocks. The same relations can be used for the well log data under examination.

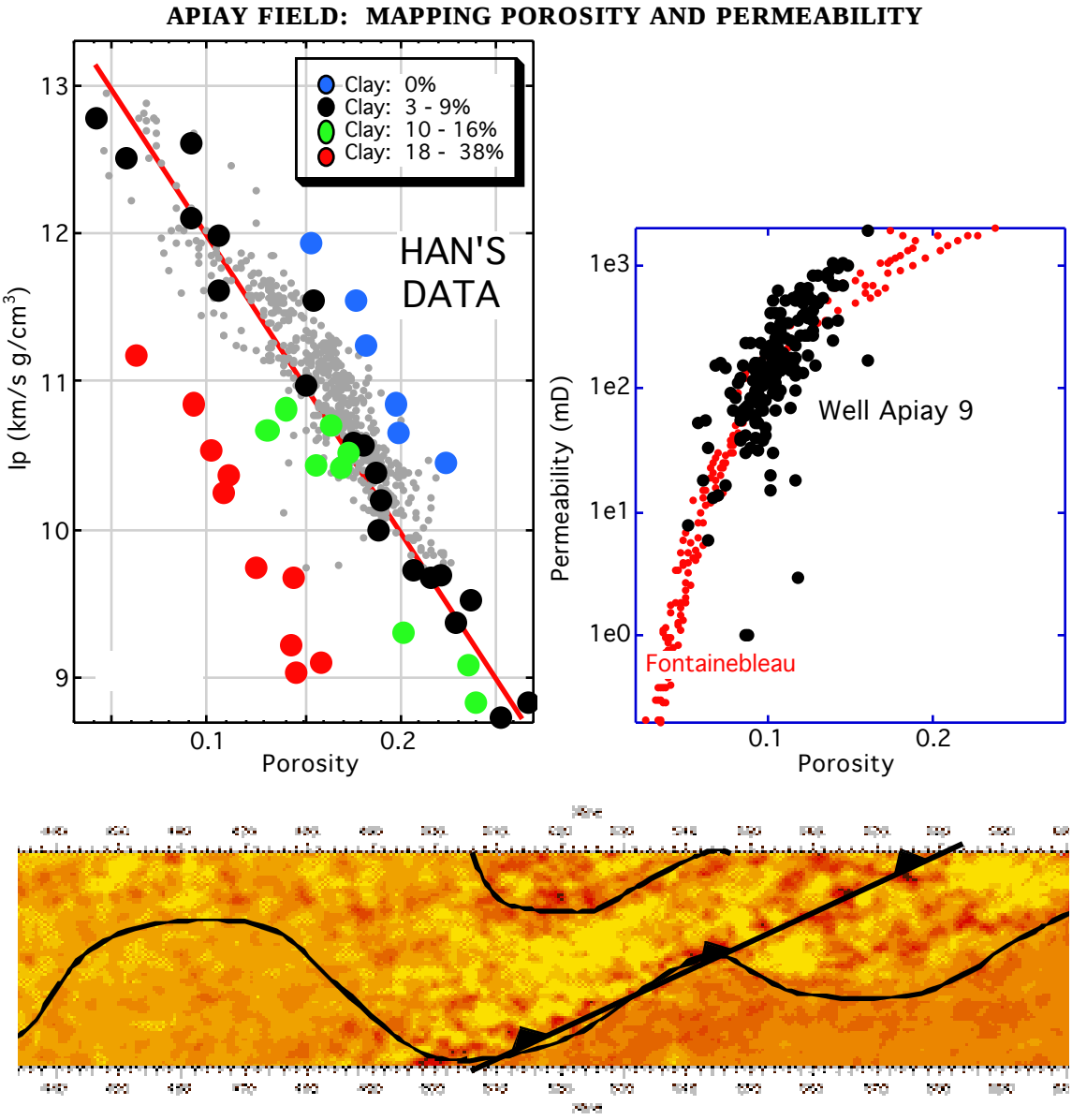

DIAGNOSTIC 3: FINDING EMPIRICAL TRENDS

STEP 1: Bring the entire interval under examination, or the suite of core data, to common pore fluid saturation. Calculate the elastic moduli at this common saturation. This step is identical to that in DIAGNOSTIC 1.

STEP 2: Cross-plot the compressional modulus at common saturation versus porosity, identify trends and relate them to specific depth intervals and depositional sequences.

We apply diagnostic approach to examining well log curves from a North Sea well. Several velocity-porosity trends are present in the well which are related to the texture.

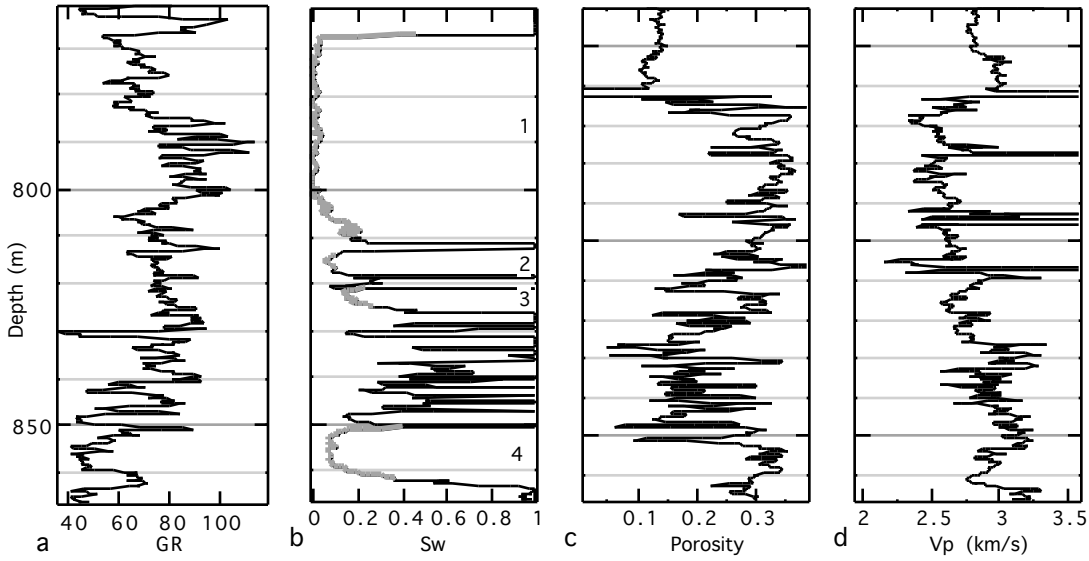

Figure 15. Gamma-ray (a), water saturation (b), porosity (c), and P-wave velocity (d) versus depth. Depth is counted not from the surface.

The gamma-ray, water saturation, porosity, and P-wave velocity curves are given in Figure 15. Porosity has been calculated from bulk density. It's values are very close to those directly measured on several core plugs. The depth interval under examination can be subdivided into four pay zones (Figure 15b). We use the velocity, porosity, and saturation data and the Vp-only fluid substitution equation to calculate the compressional modulus of the rock fully saturated with formation water. This modulus is plotted versus log-derived porosity in Figure 16.

Four data clusters are present in Figure 16. One is associated with part of the deepest Zone 4 and falls on the cementation theoretical curve (Zone 4a). Another also belongs to Zone 4 and is grouped to the left of the cementation curve (Zone 4b). The data from Zone 2 and 3 form a linear modulus-porosity trend. The data from the shallowest Zone 1 form a low-velocity, high-porosity cluster. The data points from Zone 2 and 3 do not fall on any of the theoretical lines. The observed modulus-porosity trend is probably due to deteriorating sorting. A simple linear least-square line can be calculated that will fit those data. This line can be used as a

modulus-porosity relation for rock physics transformations required in reservoir characterization.

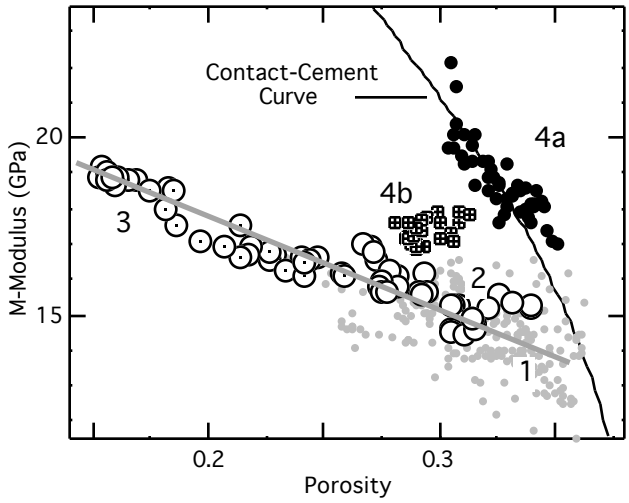

Figure 16. Compressional modulus versus porosity.

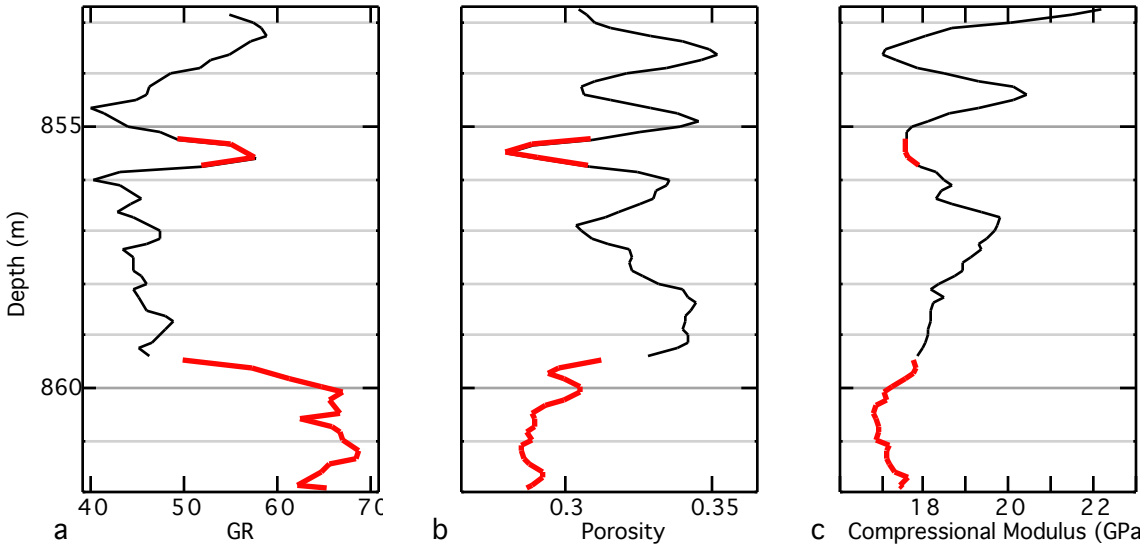

Figure 17. Zone 4. GR (a), porosity (b), and compressional modulus (c) versus depth.

Notice that a group of datapoints from Zone 4 (4b) forms a cluster in the modulus-porosity plane that is separate from the contact-cement Zone 4a trend. At a fixed porosity, the modulus in this cluster is smaller than that predicted by the contact-cement theory and larger than that in the other zones. To analyze Zone 4b, consider the gamma-ray, porosity, and compressional-modulus curves for Zone 4 only (Figure 17). The Zone 4a datapoints correspond to the thin black lines whereas those from Zone 4b are shown by the bold gray lines.

It is clear from Figure 17 that the low-velocity Zone 4b cluster correspond to the relatively high gamma-ray 2 meter long interval at the bottom of Zone 2 and to a very thin interval in the

middle. These two intervals also have relatively small porosity. Apparently here clay fills the pore space and reduces porosity without affecting the stiffness of the contact-cemented frame.

EXAMPLE 1 OF ROCK PHYSICS DIAGNOSTIC:

COMPETING EFFECTS OF SATURATION AND ROCK TEXTURE

SUMMARY

In this example we analyze an interval in a vertical North Sea well that intersects oil-water and gas-oil contacts. Velocity in the gas zone appears to be higher that in the oil- and water zone, in spite of the high total porosity. This section of the interval corresponds to the constant and relatively low GR values. Therefore, this high-velocity effect is due to the texture of rock in the gas zone that is most likely to be connected with the depositional environment.

INTRODUCTION AND PROBLEM FORMULATION

It is generally expected that velocity in gas-saturated rock is smaller than in rock saturated with oil or water. However, in the well under examination, the opposite is true: the P-wave velocity increases across the gas-oil contact being larger in the gas zone (Figure 1b). This is in spite of the total porosity in the gas zone being much larger than porosity in the oil and water zones (Figure 1d). Our goal is to resolve this apparent inconsistency by the means of rock physics diagnostic.

SOLUTION VIA ROCK DIAGNOSTIC

Notice that in the well under examination, a low-GR (about 75 API) interval starts just above GOC and ends at about 1.53 km depth. In contrast, gamma-ray values between GOC and OWC reach 125 API. The low-GR interval corresponds to relatively high P-wave velocity (2.4 km/s) and high porosity (33% - 35%). Velocity above GOC is higher than below GOC. The shear-wave velocity also exceeds that below the gas-oil contact. This observation tells us that in addition to pore fluid, rock fabric may be also responsible for velocity-depth variations.

To approach this task we have to diagnose rocks in the interval under examination. To do so, we have to determine the elastic constants and densities of pore fluid components. We determine these properties using the Batzle-Wang (see in Mavko et al., 1998) formulas for reservoir temperature 70 ^{o}C and pore pressure 16 MPa. The results are given below.

Estimates for Pore Fluid Properties

Fluid	Density (g/cm^3)	Bulk Modulus (GPa)	Gravity (API)	Salinity (ppm)
Water	1.024	2.72		56,000
Oil	0.68	0.6	40 (GOR = 150)	
Gas	0.116	0.03	0.6	

The sonic data come from dipole measurements. We assume that there is no mud-filtrate invasion effect on the dipole and density data because porosity is high and, therefore, the invasion radius has to be small.

Therefore, we use the virgin saturation data to calculate the bulk modulus of the pore fluid that is a mixture of water, oil, and gas. When doing so, we assume that there is no oil above GOC and no gas below it. Obviously, such an assumption approximates the real situation. These fluid properties are used to calculate the compressional modulus in the interval at 100% water saturation.

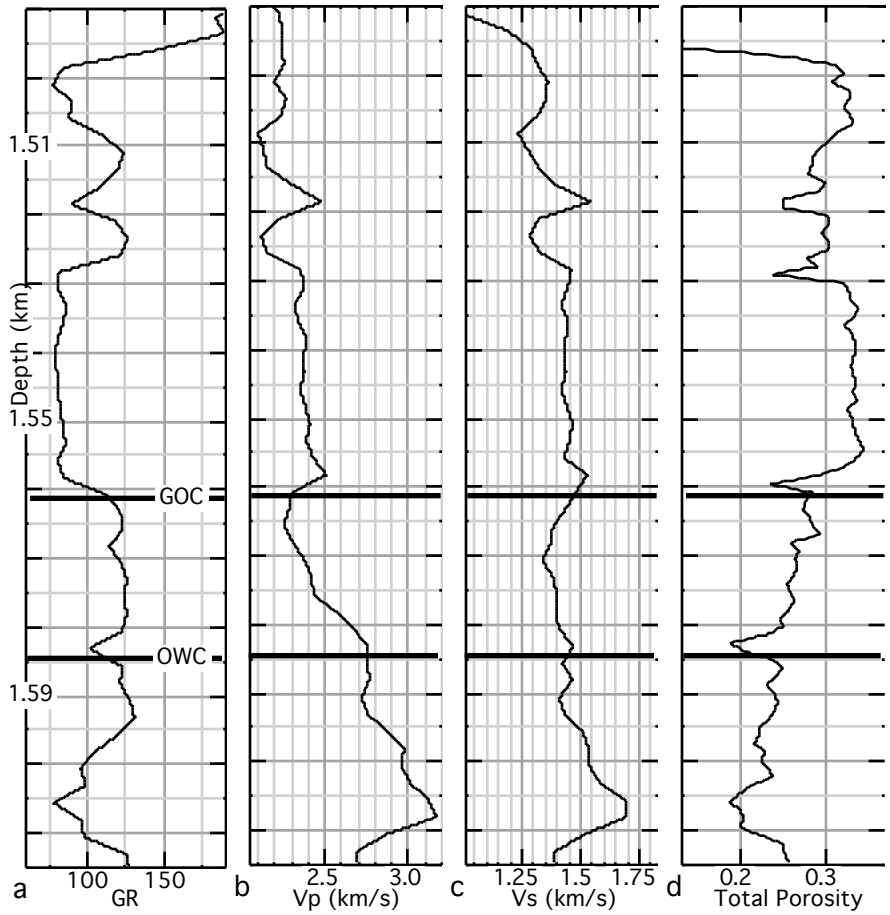

Figure 1. Gamma-ray, velocity, and total porosity versus depth. Velocity in the gas-saturated zone is higher than below it.

Let us cross-plot the compressional (M) modulus versus porosity for the entire interval under examination (Figure 2a). The water and oil zones show clear modulus-porosity trends. The gas zone shows two trends: one for the interval above 1527 m, and the other for the interval between 1561 m and 1527 m. Notice that the latter interval corresponds to low gamma-ray readings (Figure 3).

In order to be able to compare gas to oil to water intervals, we theoretically resaturate the entire interval with 100% formation water. We crossplot the resulting compressional modulus versus porosity in Figure 2b. All parts of the interval, except the low-GR interval in the gas

zone between 1561 m and 1527 m appear to be on the same modulus-porosity trend that is the unconsolidated theoretical line of Dvorkin and Nur (1996). The low-GR gas interval stands out and lies on a constant-cement line (Avseth et al., 1998) with very small amounts of contact cement.

The shear-modulus crossplot (Figure 4) further supports this hypothesis.

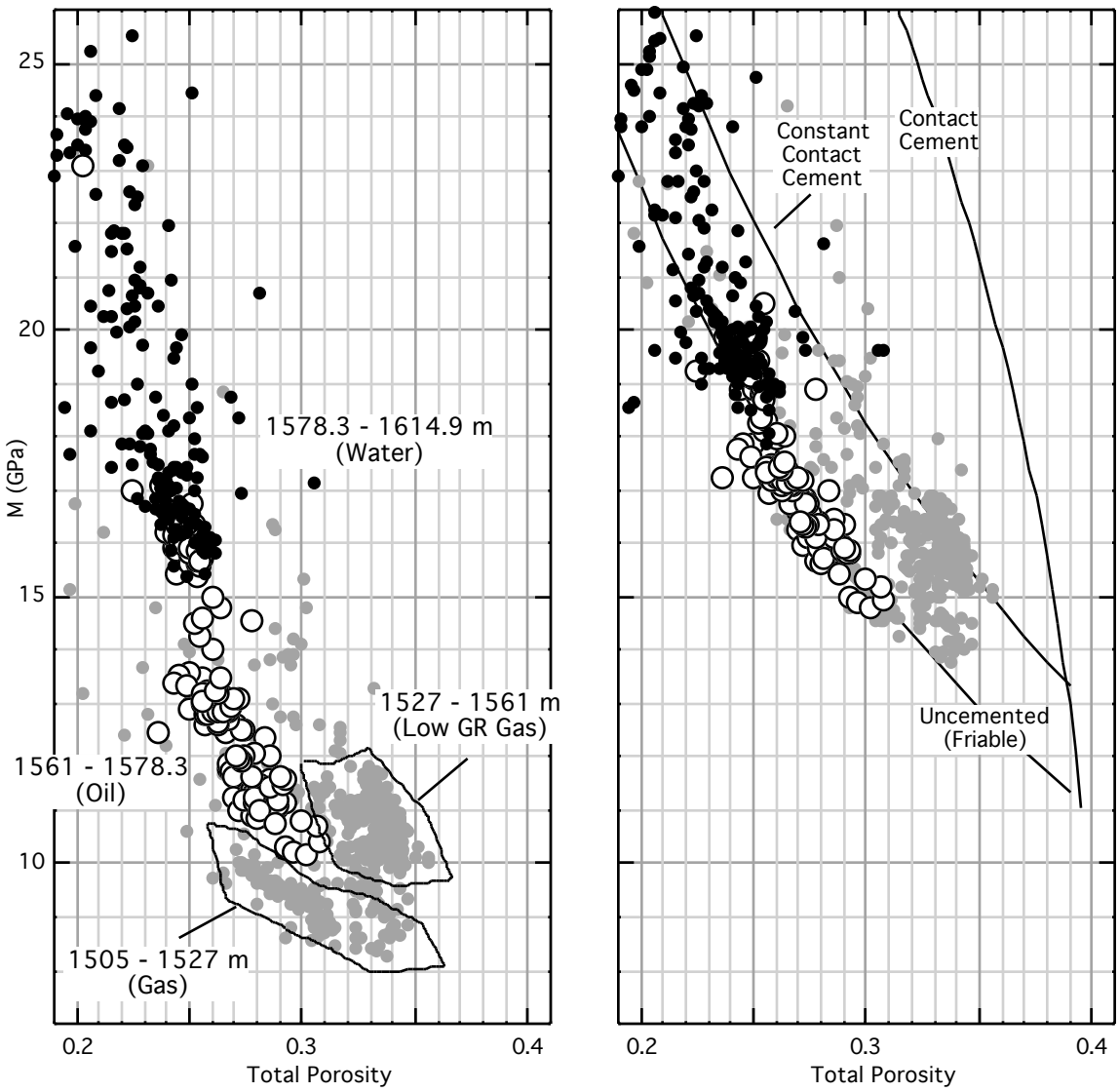

Figure 2. Compressional-modulus versus porosity below OWC, between OWC and GOC, and above GOC. Left: modulus as measured; right: modulus with uniform saturation (100% brine) with superimposed theoretical curves.

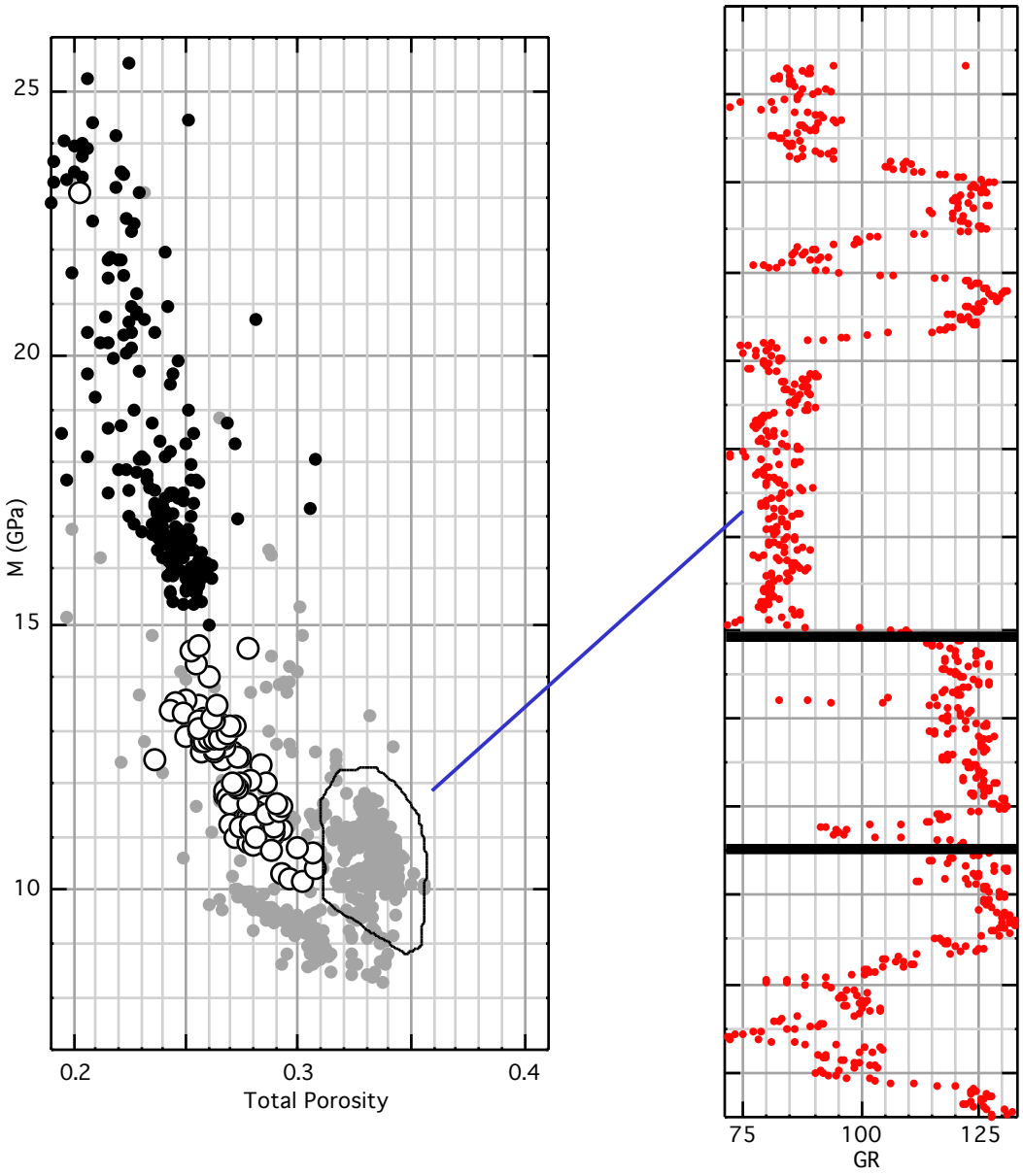

Figure 3. Anomalous velocity data correspond to the low-GR interval in gas zone.

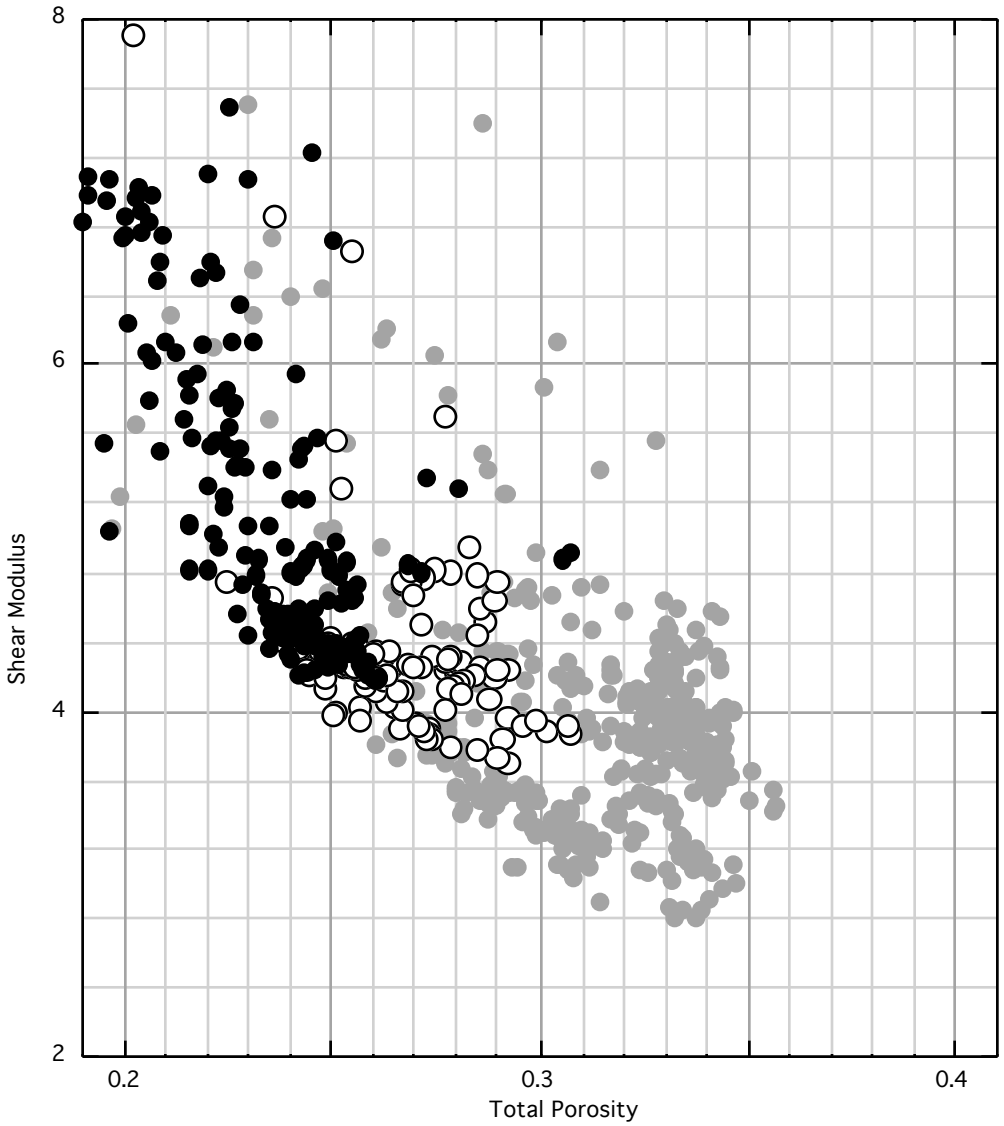

Figure 4. Shear modulus versus porosity. Symbols are same as in Figure 3.2.

CONCLUSION

We conclude that it is rock texture rather than pore fluid that is responsible in this case for the observed vertical velocity variations and contrasts.

The thin section images (Figure 5) do not directly show the presence of contact cement. However, the apparent angularity of the coarse grains corresponding to the low-gamma-ray gas-filled interval may indirectly indicate the presence of slight contact cementation.

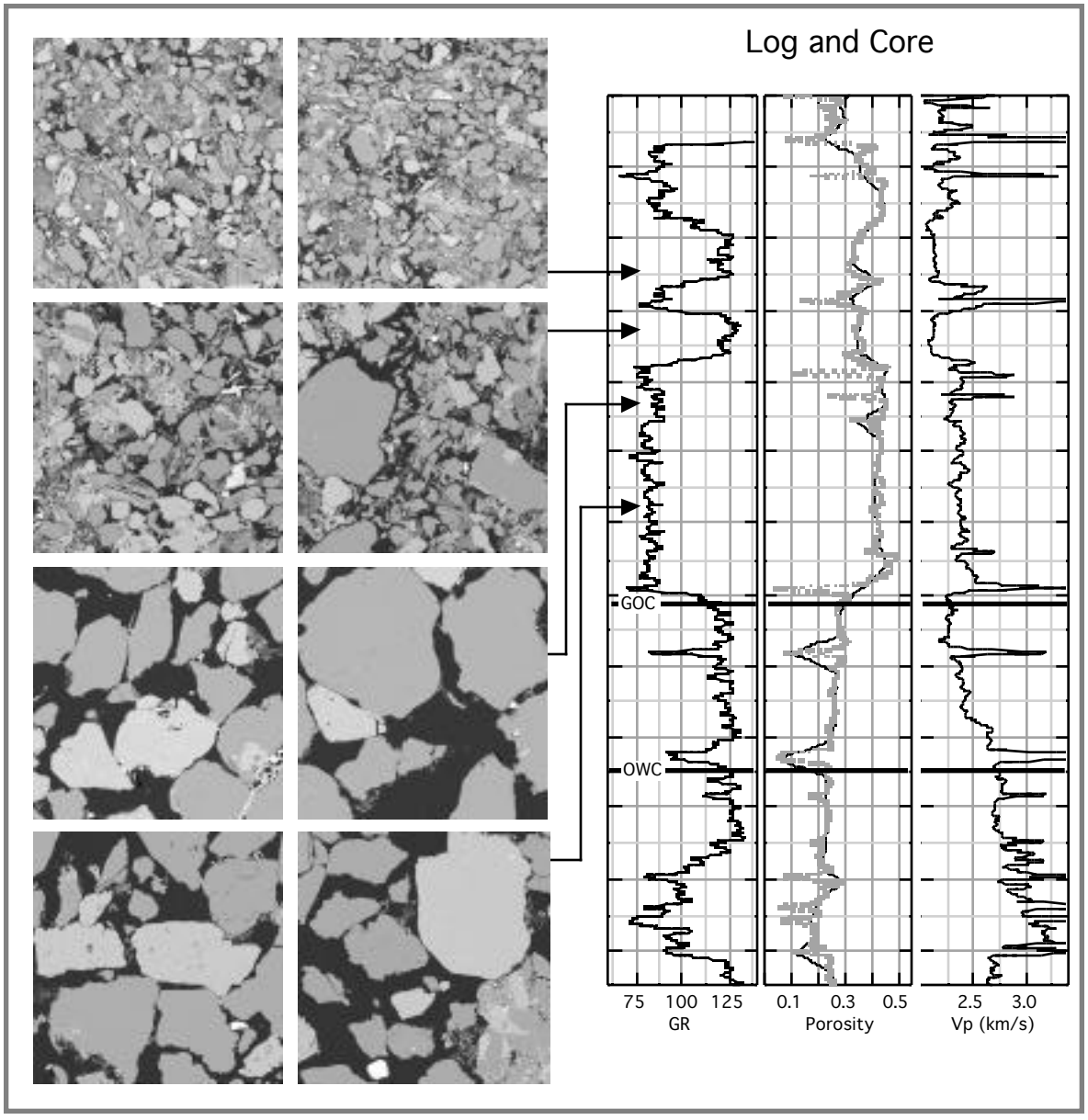

Figure 5. Thin sections and corresponding depth intervals.

EXAMPLE 2 OF ROCK PHYSICS DIAGNOSTIC:

STRENGTH AND PERMEABILITY FROM POROSITY AND VELOCITY FOR HIGH-POROSITY SANDSTONES

SUMMARY

In high-porosity sandstones, permeability depends not only on porosity, but also on the location of the pore-filling minerals. It is affected mostly by the part of the pore-filling cement that is deposited away from grain contacts and clogs the pore space. On the other hand, the elasticity of sandstones (which determines the elastic-wave velocity) is affected mostly by the rest of the cement, i.e., by its part deposited at grain contacts. Then, by analyzing velocity data, one can estimate the volume of the contact cement. Once this quantity is known, porosity can be used to find the volume of the remaining, non-contact, cement whose effect on permeability is large. We offer a new rock physics theory to quantify the amount of the non-contact cement in sandstones from dry-rock velocity and porosity data. We apply this theory to field well-log data and show that by relating permeability to the volume of the non-contact cement a meaningful trend can be achieved, with much less scatter than the corresponding permeability-porosity trend. This success renders viable the approach where sonic and porosity logs are used together to diagnose the rock for its pore-scale structure and, based on this diagnostic, quantify properties that cannot be measured directly.

INTRODUCTION

Non-uniqueness in relating velocity to porosity in core and well-log data complicates interpretation of sonic and seismic measurements. One reason for this non-uniqueness in sandstones is clay (e.g., Han, 1986). Another reason is textural variability among samples. Dvorkin and Nur (1996) examine two relatively clay-free sandstone groups in the same porosity range, but whose velocities significantly differed (Figure 1a). By comparing the data with effective-medium theories they interpret this velocity difference as resulting from the difference in the position of diagenetic cement. The explanation is that in the "fast" (Oseberg) rocks (contact) cement is located predominantly at the grain contacts whereas in the "slow" (Troll) rocks (non-contact) cement is located predominantly away from these contacts.

Coincidentally, the permeability of the Troll rocks is smaller than that of the Oseberg rocks (Figure 1b). This fact allows us to assume that the position of the diagenetic cement affects not only velocity but also permeability. The assumption is supported by numerical simulations of Bosl et al. (1998). This effect has a simple physical explanation: the non-contact cement acts to increase the specific surface area (Figure 1b) and thus decrease permeability.

Consider now a dataset where a clear trend between porosity and permeability is absent. Our working hypothesis is that this may be due to the variability in the location of diagenetic

cement. We use this hypothesis in a case study where permeability and porosity data are available from cores in a well and velocity is available from a sonic log. A relationship between permeability and porosity is absent. The goal is to find a textural property of high-porosity sandstones with which permeability correlates well.

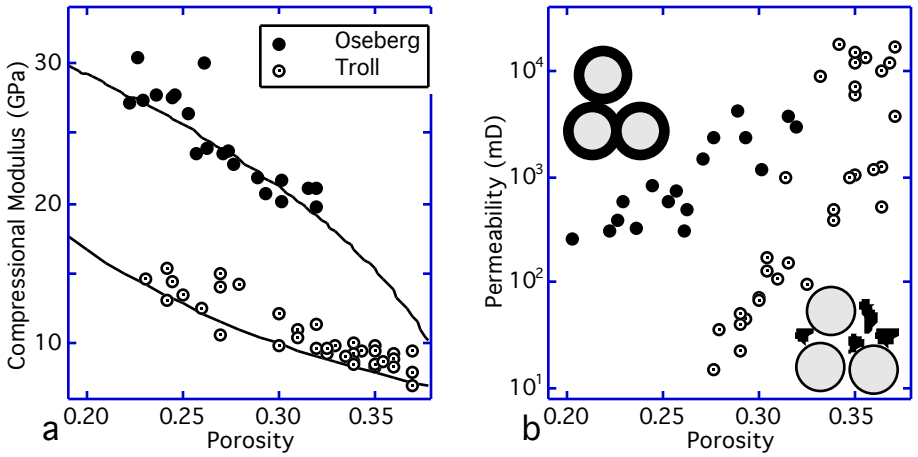

Figure 1. a. Compressional modulus (the product of bulk density and P-wave velocity squared) versus porosity for the Oseberg and Troll samples. The data displayed are for room-dry rocks at 30 MPa effective pressure (Strandenes, 1991; and Blangy, 1992). The upper curve is from the contact cement theory and the bottom curve is from the non-contact cement theory (Dvorkin and Nur, 1996). b. Permeability versus porosity for the same datasets (Strandenes, 1995). The cartoons schematically show the location of cement among grains (contact for Oseberg and non-contact for Troll).

NORTH SEA SLEIPNER FIELD, WELL 15/9-16

A vertical well, 15/9-16, penetrates the North Sea Sleipner gas/condensate reservoir comprised of Paleocene turbiditic sand. Porosity and permeability are available from about 60 plugs that evenly cover the interval from 2380 to 2460 m. The vertical and horizontal permeabilities are practically identical. The sandstone is very well sorted. The grains are predominantly quartz (average 80%) with the rest being feldspar (average 14%), mica (average 2.3%), and clay, mostly chlorite, (average 2.2%). Traces of calcite and other minerals are also present. The contact cement in these rocks is quartz (Nadeau, 1998).

The upper part of the well is saturated with gas, with the gas-water contact at 2430 m. The bulk moduli and densities of the formation water and gas are 2.75 GPa and 1.02 g/cm^3, and 0.07 GPa and 0.27 g/cm^3, respectively (following Batzle and Wang, 1992).

The interval under investigation can be subdivided into a high-resistivity zone (HRZ) overlaying a low-resistivity zone (LRZ) with the transition at about 2410 m (Figure 2a). Nadeau (1998) shows that there is a diagenetic change associated with this transition. HRZ has a restricted distribution of diagenetic chlorite and up to 5% quartz cement. LRZ has a slightly larger content of chlorite and a smaller degree of cementation.

Porosity in the entire interval is high. We calculate it from bulk density (Schlumberger, 1989). It's values do not differ much from those measured on cores except for a few points in LRZ (Figure 2b). The final results of this study practically do not depend on what porosity (log-derived or core) we use. For this reason we relate all parameters to the log-derived porosity.

The available log data contain only compressional-wave velocity. We calculate the dry-frame compressional modulus (the product of bulk density and P-wave velocity squared) by the V_p-only fluid substitution method of Mavko et al. (1995). The result is well matched by the values measured on several selected room-dry plugs (Figure 2d). The 30 MPa effective pressure for these datapoints essentially equals the reservoir effective pressure (about 29 MPa).

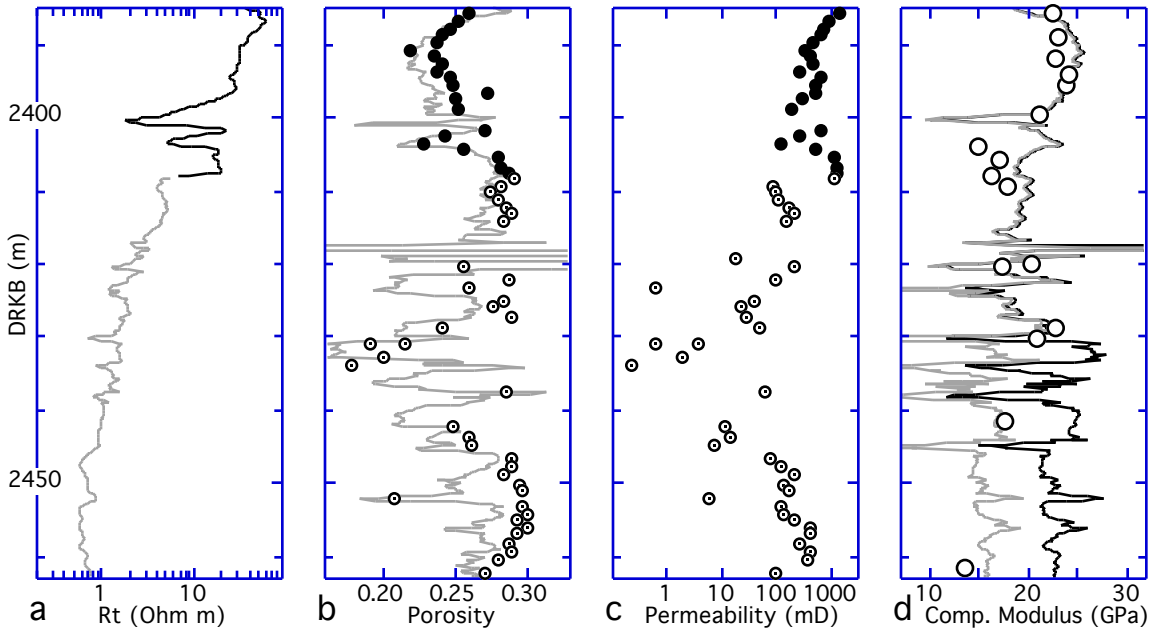

Figure 2. Various parameters versus depth in well 15/9-16. a. Far resistivity. Gray curve is for LRZ. b. Log-derived (gray curve) and core porosity. Open symbols are for LRZ. c. Permeability. Open symbols are for LRZ. d. Dry-rock (gray curve) and directly measured (black curve) compressional modulus. Symbols are from dry-rock lab measurements at 30 MPa.

ANALYSIS OF DATA

There is a very weak correlation between permeability and porosity (either log-derived or core) in well 15/9-16 (Figure 3). This fact can also be observed in Figures 2b and 2c where porosity and permeability are plotted versus depth. The lower-porosity sandstones in HRZ have permeability larger than that of the higher-porosity sandstones in LRZ. Notice also that the LRZ sandstones are softer than the HRZ sandstones (Figure 2d).

The modulus-porosity and permeability-porosity trends for HRZ and LRZ are given in Figure 4. In the modulus-porosity plane (Figure 4a) the HRZ trend parallels that of the contact-

cemented Oseberg rocks and the contact cement theoretical trajectory (the latter calculated for quartz grains with quartz cement). The HRZ rocks have a tight modulus-porosity trend. Remarkably, in the permeability-porosity plane (Figure 4b) the HRZ sandstones plot on top of the Oseberg data and also exhibit a noticeable permeability-porosity trend.

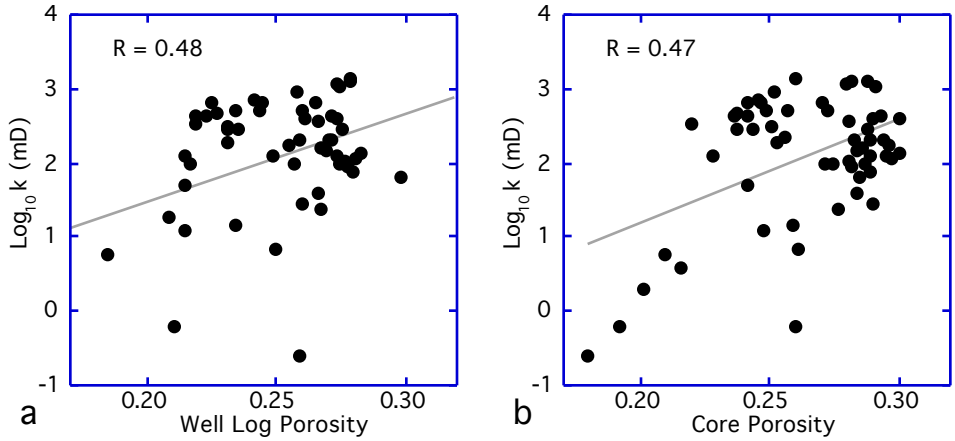

Figure 3. Horizontal permeability versus log-derived (a) and core (b) porosity. Gray lines show best linear fits. Correlation coefficients are given in the graphs.

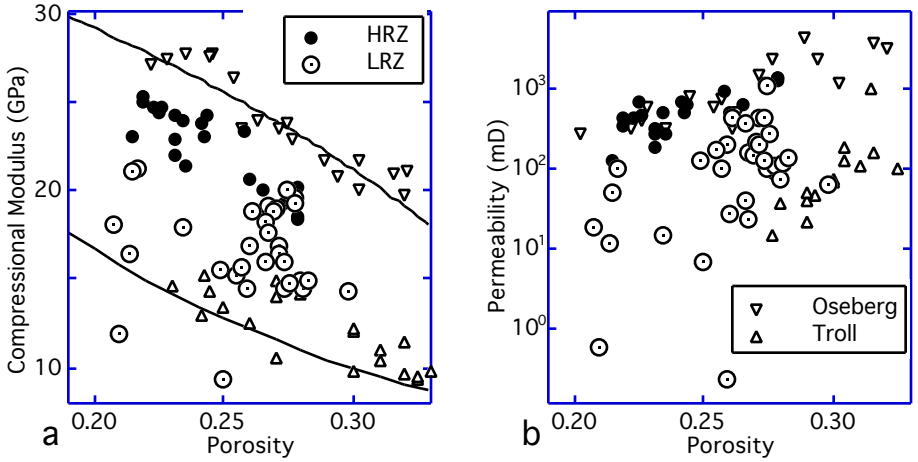

Figure 4. a. Dry-frame compressional modulus versus porosity for the Oseberg and Troll samples at 30 MPa, and HRZ and LRZ. The HRZ and LRZ data are selected at the depths of permeability datapoints. The upper curve is from the contact cement theory and the bottom curve is from the non-contact cement theory. b. Permeability versus porosity for the same datasets. The open triangles are for Oseberg and Troll. The filled circles are for HRZ and the open circles are for LRZ. The Oseberg and Troll data are plotted versus core porosity whereas the HRZ and LRZ data are plotted versus log-derived porosity.

The LRZ sandstones on the other hand do not show a modulus-porosity trend. These datapoints fill the space between the contact and non-contact cement theoretical trajectories (the latter calculated for quartz rock at 29 MPa effective pressure). Similarly, in the permeability-porosity plane these rocks fill the space between the Troll and Oseberg datapoints, and a permeability-porosity trend is absent.

As we mentioned before, both HRZ and LRZ rocks are quartz-cemented and have very close mineralogy. Based on these facts, we assume that both the modulus-porosity and permeability-porosity non-uniqueness (Figure 4) is due to the varying amounts of contact and non-contact cement.

DIAGNOSING ROCK FOR NON-CONTACT CEMENT

In order to calculate the amount of the non-contact cement from sonic and porosity we use a model where a high-porosity sandstone has an idealized texture. Its basic framework is a random dense pack of identical spherical grains at some critical porosity ϕ_c which may vary between 0.36 and 0.4. Every grain is identically and evenly enveloped by a layer of contact cement, and the rest of the solid phase (additional to the grains and contact cement) forms non-contact cement deposited in the pore space away from grain contacts (Figure 5a).

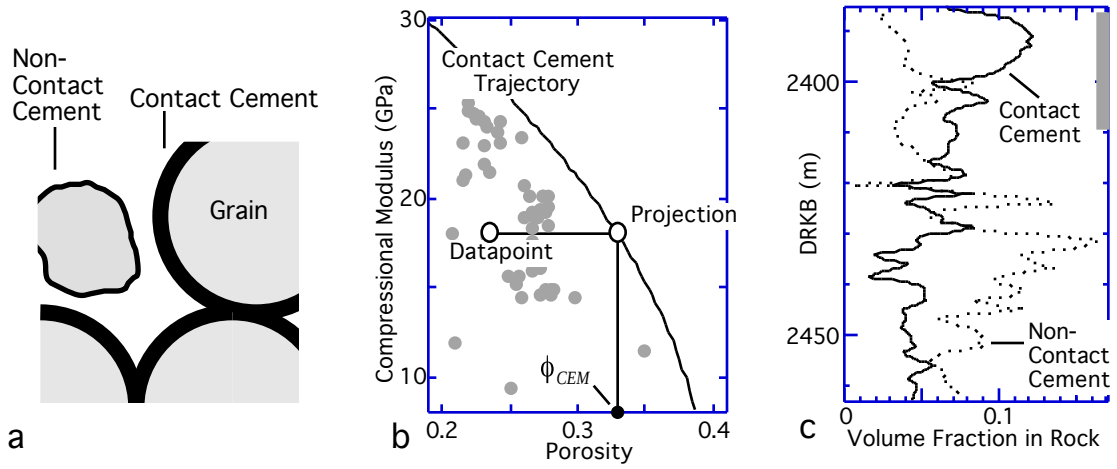

Figure 5. a. Idealized picture of granular rock with contact and non-contact cement. b. Calculating the amount of non-contact cement. Gray symbols show some scattered datapoints. c. Volumetric fraction of contact (solid line) and non-contact (dotted line) cement versus depth in well 15/9-16. Gray vertical bar shows the extent of HRZ.

Let us now consider a datapoint in the modulus-porosity plane that lies below a theoretical contact cement trajectory (Figure 5b). We assume that the non-contact cement does not contribute to the stiffness of this rock. Therefore, its elastic modulus is identical to that of a higher porosity (ϕ_{cem}) rock of the same texture but without the non-contact cement. The corresponding datapoint is the horizontal projection (in the modulus-porosity plane) of the original one onto a contact-cement trajectory (Figure 5b).

Volume balance gives the following relations between the porosity of the datapoint (ϕ), its projection on the contact-cement trajectory (ϕ_{cem}), critical porosity (ϕ_c), and the volume fractions of the contact (f_{cc}) and non-contact (f_{ncc}) cement in rock:

$$f_{cc} = \phi_c - \phi_{cem};\ f_{ncc} = \phi_c - \phi - f_{cc}.$$

The contact-cement trajectory can be plotted using equations in Dvorkin and Nur (1996); it depends on the elastic moduli of grains and cement, and on the chosen critical porosity value. An additional input parameter is the average number of contacts per grain in the original sphere pack (n). It may vary between 9 and 8.

In the case under examination we choose ϕ_c = 0.38 (average between 0.36 and 0.4) and n = 8.5. Because the grains and contact cement are predominantly quartz, we plot the contact-cement trajectory for quartz-cemented quartz grains (Figure 4.5b). In calculating this trajectory, we use 38 GPa and 44 GPa for the bulk and shear moduli of quartz, respectively.

This trajectory can be fitted (with correlation coefficient about 1) by the equation

$$1.037\sqrt{0.38-\phi_{cem}} = -0.0013 + 0.0134M + 4.3\ 10^{-5}M^2,$$

where M is the compressional modulus of the dry contact-cemented rock.

Now we can combine the above equations to relate the volumetric fractions of the contact and non-contact cement to the dry-frame compressional modulus and porosity:

$$f_{cc} = 0.93(-0.0013 + 0.0134M + 4.3\ 10^{-5}M^2)^2,\ f_{ncc} = 0.38 - \phi - f_{cc}.$$

These fractions, as calculated for well 5/9-16 (using the dry-frame compressional modulus from fluid substitution) are given in Figure 5c. The contact cement dominates in HRZ whereas the non-contact cement is prevalent in LRZ.

This diagnostic can be immediately used to assess the strength of the rock: clearly the larger the amount of contact cement the stronger the rock (at the same porosity). This effect could be clearly seen in the Troll and Oseberg example (Figure 1). The Troll samples that do not have contact cement are friable sands (Blangy, 1992), whereas the Oseberg samples show significant structural integrity (Strandenes, 1991). In this case, our diagnostic is also consistent with the rock's strength: Nadeau (1998) states that quartz cementation progressed more readily in HRZ and is associated with intervals less prone to sand production.

PERMEABILITY TREND

In Figure 6a we plot the logarithm of permeability (k) versus the volumetric fraction of the non-contact cement. A linear trend is evident (as opposed to the absence of such in Figure 3). The linear-fit equation for this trend is $\mathrm{Log}_{10}k = 3.3 - 19.46\,f_{ncc};\ R = 0.85$.
The correlation slightly improves if the permeability is normalized by the grain size (d) squared (Figure 6b): $\mathrm{Log}_{10}(k/d^2) = 4.8 - 20.47\,f_{ncc};\ R = 0.86$. Such normalization is often used to improve permeability trends because permeability strongly depends on the grain size (e.g., Bourbie et al., 1987). In our case this improvement is small due to a relatively uniform grain size distribution in the interval (between 0.15 and 0.25 mm).

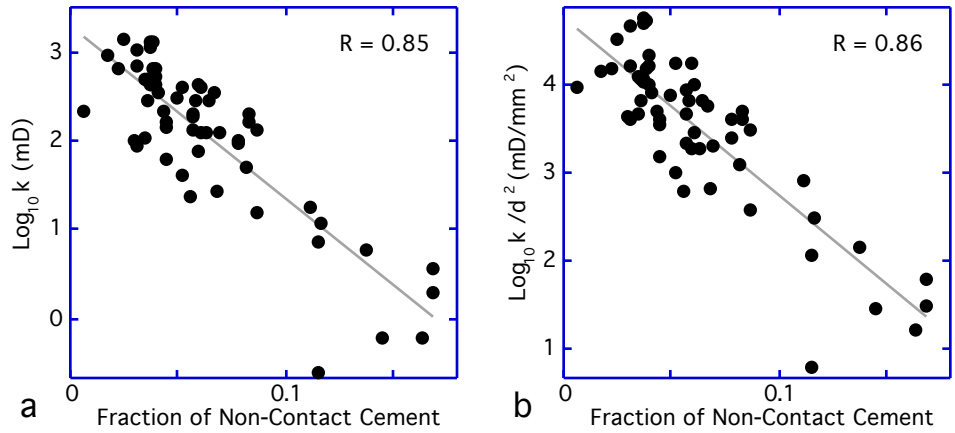

Figure 6. Permeability (a) and permeability normalized by grain size squared (b) versus the volumetric fraction of non-contact cement. Gray lines show best linear fits. Correlation coefficients are given in the graphs.

The method of calculating the amount of contact and non-contact cement presented here is in fact a method of diagnosing the texture of high-porosity sandstone from well-log data. Such diagnostic is important not only for obtaining a usable correlation for permeability but also for assessing the strength of rock and its susceptibility to sanding.

EXAMPLE 3 OF ROCK PHYSICS DIAGNOSTIC: DIAGNOSING HIGH-POROSITY SANDS FOR RESERVOIR CHARACTERIZATION USING SONIC AND SEISMIC

SUMMARY

At high porosity, velocity in reservoir rocks strongly depends on the position of the intergranular material. Velocity is high if the original grains are cemented at their contacts. It is low if the pore-filling material is placed away from the contacts. In the latter case we have truly unconsolidated sediments. In the former case we have high-porosity cemented rocks. Separating these two rock types is important for hydrocarbon identification.

Due to the difference in the rock frame stiffness between the unconsolidated and high-porosity cemented rocks, seismic signatures of the former filled with water can be very close to those of the latter filled with hydrocarbons. This may complicate direct hydrocarbon detection. We separate the two rock types by diagnosing sand using rock physics theory.

We conduct such diagnostic on well log data from two wells that penetrate the Heimdal formation (North Sea). We show that the Heimdal formation reservoir is composed of both unconsolidated and cemented high-porosity sands. The initial quartz cementation present in the latter is clearly seen in the cathode-luminescent SEM images. These images, combined with point XRD analysis, confirm our diagnostic that the high-velocity high-porosity sands in Heimdal contain quartz grains surrounded by quartz-cement rims.

We find that the two different types of sand which are capped by similar low-impedance shales produce drastically different AVO signatures. The oil-filled high-porosity cemented sand shows a relatively strong zero-offset reflectivity which becomes less positive with increasing offset, while the oil-filled uncemented sand shows a negative zero-offset reflectivity with increasingly negative far-offset response.

These results show that (1) rock diagnostic can be conducted not only on the log scale but also on the seismic scale; and (2) taking into account the nature of the rock improves our ability to identify pore fluid from seismic.

ROCK DIAGNOSTIC AND CONFIRMATION

We examine two wells -- Well #1 and Well #2. Sonic velocity and gamma-ray are plotted versus depth for both wells in Figures 1a to 1d. Vp is plotted versus porosity in Figures 1d and 1f. Notice that in Well #2 a thick sand interval (gray bar in Figure 1c) is marked by extremely low and constant gamma-ray readings. This sand layer is surrounded by high-gamma-ray shale packages. In Figure 1f, these two lithologies fall into two distinctive velocity-porosity patterns. In Well #1, unlike in Well #2, we observe a gradual variation of clay content between very clean sand and shale. Only a relatively thin (10 m) sand interval (gray bar in Figure 1a) is identified as a practically clay-free reservoir sand. Because of the gradual

variation of clay content in this well, we do not observe (Figure 1e) velocity-porosity patterns as distinctive as in Well #1. These two clean sand intervals (in both wells) represent the same stratigraphic level, although located in different oil fields. They are shown by bold black symbols in Figures 1e and 1f.

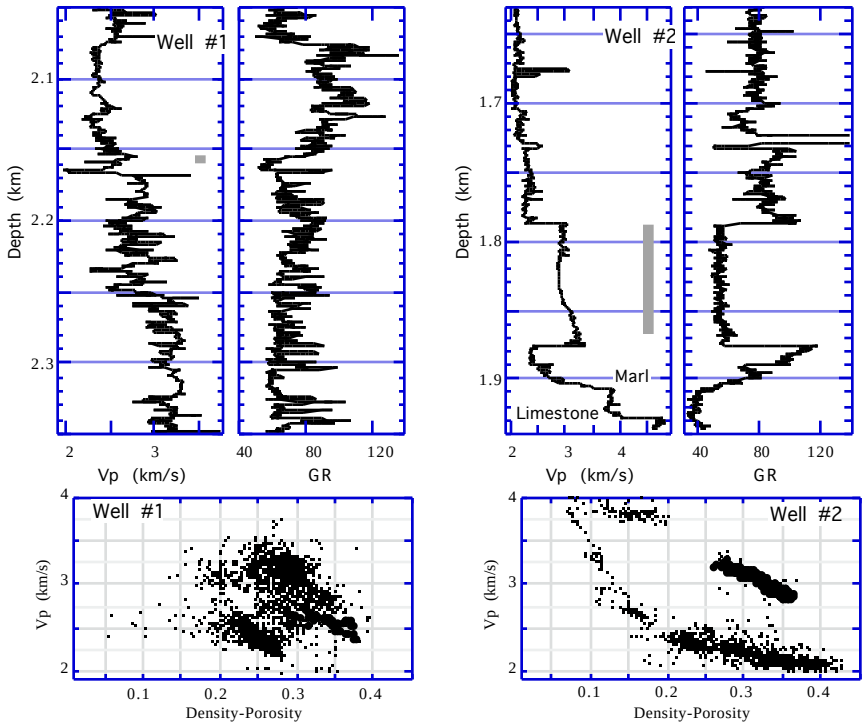

Figure 1. P-wave velocity and gamma-ray versus depth (a-d); and P-wave velocity versus porosity (e and f) for both wells.

For the purpose of diagnostic, we plot together these two subsets of the data (Figure 2). We diagnose these rocks by superimposing theoretical rock physics curves (Dvorkin and Nur, 1996) on this plot. The contact cement line corresponds to the case where rock is formed by quartz-cement rims growing on sand grains. Here velocity drastically increases with only slightly decreasing porosity. The unconsolidated line corresponds to the case where porosity reduces not due to the growth of contact cement, but due to loose pore-filling material such as small grains, mica and detrital clay particles. Here velocity strongly depends on the effective pressure (about 20 MPa here) and only gradually increases with decreasing porosity. Notice that the Well #2 data points do not fall on the contact cement line. This is because the volumetric fraction of contact cement in these rocks, according to a thin section point-count analysis, is constant (about 2%) in the entire porosity range. Therefore this contact cement is responsible for the initial drastic velocity increase (as compared to uncemented sand) at 37% porosity, but the continuing porosity decrease is due to loose pore-filling material. This concept is represented by the constant cement fraction line that has the shape of the

unconsolidated line, but a different high-porosity end member. The two sand intervals can be diagnosed by rock physics theory as: (a) Well #1 -- unconsolidated quartz sand; and (b) Well #2 -- contact-cemented quartz sand with a constant fraction of cement in the whole rock.

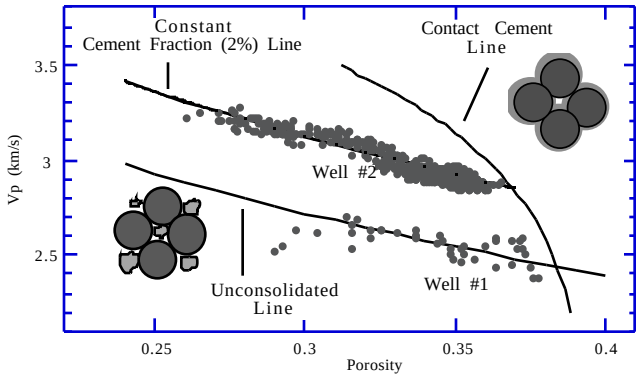

Figure 2. P-wave velocity versus porosity for sand intervals in both wells. Theoretical lines serve to diagnose the rocks.

To directly confirm this diagnostic, consider the thin sections of two samples from both intervals (Figure 3). The samples have approximately same porosity. They are predominantly quartz. No contact cementation is apparent in both images. The left image (Well #1) shows some organic coating around quartz grains. Consider now two SEM images of a sample from Well #2 (Figure 4). The left-hand image is in back-scatter light and the right-hand one is in cathode-luminescent light. Notice the V-shaped grain in the middle. No contact cement rim is apparent around this grain in back-scatter light. Cathode-luminescent light reveals a contact-cement rim around this grain. The point XRD analysis shows that both the grain and cement rim are pure quartz. This confirms our diagnostic that the Well #2 sand interval is contact-cemented. The hexagonal crystal shapes in the upper left corner also indicate diagenetic cementation. No cement rims or hexagonal crystal shapes have been found around grains in the sand interval from Well #1. Another direct proof of our diagnostic was that cores extracted from Well #1 appeared as piles of loose sand, whereas those from Well #2 supported external stress.

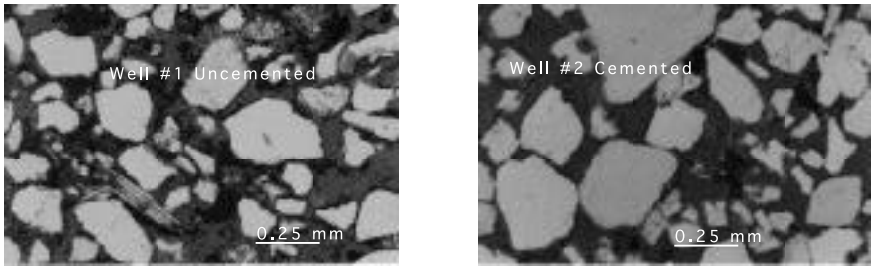

Figure 3. Thin sections of two selected samples from Well #1 (left) and #2 (right).

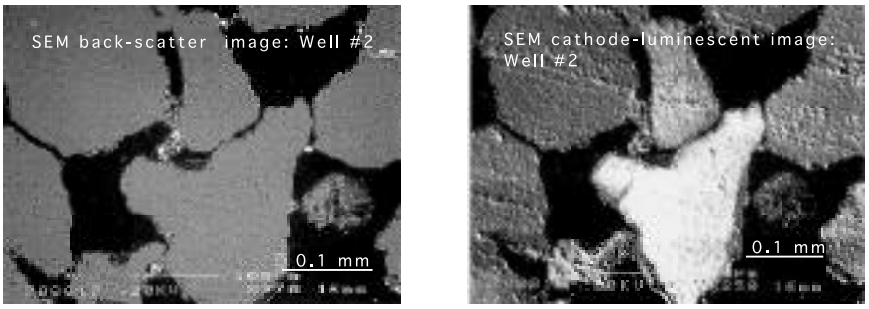

Figure 4. SEM images of a Well #2 sample in back scatter light (left) and cathode-luminescent light (right).

SEISMIC RESPONSE

To understand how the type of sand (unconsolidated versus cemented) affects the seismic response, we analyze CDP gathers at the well locations. Figure 5a shows the real CDP gather at Well #1 where the picked horizon is at the top of the Heimdal formation.

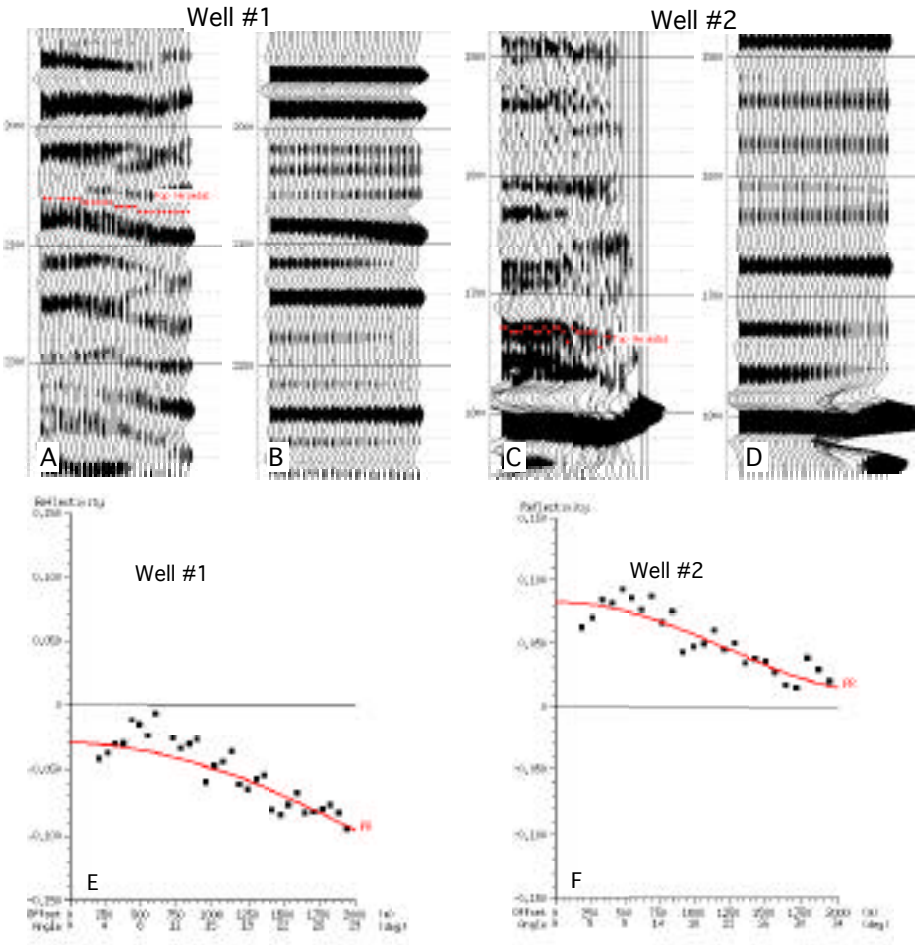

Figure 5. Top. Real (a and c) and synthetic (b and d) CDP gathers. In synthetic gathers, the AVO effect was modeled only at the target zones. Bottom. Real reflectivity versus offset and angle (symbols) and theoretical Zoeppritz lines.

Figure 5b gives a synthetic CDP gather for this well produced by using a 30 Hz zero-phase Ricker wavelet and a log-derived reflectivity series. Both the real and synthetic gathers show reflectivity increasingly negative with increasing offset at the picked horizon. This reflectivity is plotted versus offset (angle), together with the theoretical Zoeppritz line, in Figure 5e. Contrary to Well #1, the top of the Heimdal formation in Well #2 (which is capped by similar shales) produces a strong positive reflector with reflectivity decreasing with increasing offset (Figures 5c and 5d). For this well, the reflectivity is plotted versus offset (angle), together with the theoretical Zoeppritz line, in Figure 5f. The synthetic response is very close to the real data in both wells which means that we can rely on well-log-based rock diagnostic to predict seismic response.

This offset-dependent reflectivity analysis shows that clean sands of the same formation, similar porosity, and with comparable oil saturation produce drastically different seismic response depending on whether they are truly unconsolidated or have initial quartz cementation. Therefore, we can use both normal-incidence and offset-dependent reflectivity to diagnose rock and characterize a reservoir from seismic. Such rock diagnostic may be of great importance because if high-porosity contact-cemented sands are not separated from truly unconsolidated sands, one may misinterpret a change in seismic signatures caused by this petrographic effect as a pore-fluid effect.

AVO EFFECT AND PORE FLUID

It is very important to diagnose the texture of the rock not only for the purpose of strength estimation but also for reducing the risk of fluid identification from AVO data.

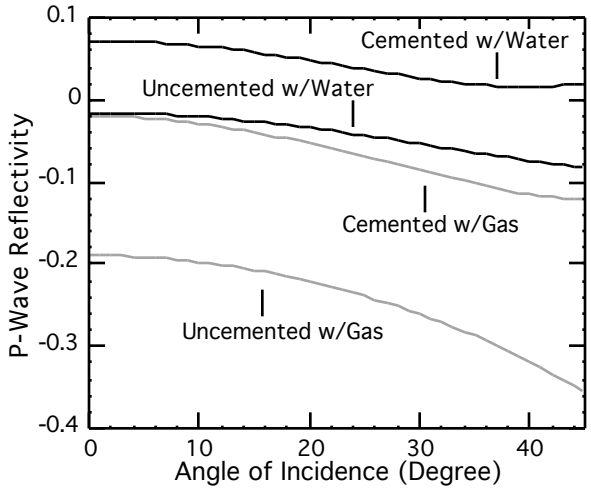

Figure 6. AVO signatures of sandstones with two different textures saturated with gas and water.

In Figure 6 we plot synthetic amplitude-versus-offset curves for a contact cemented and uncemented sandstone samples from the two wells under examination. We use Gassmann's fluid substitution equation to calculate the effective elastic properties of the samples with gas and water. In this model, the samples are overlaid with a shale layer.

We can see from Figure 6 that the AVO signature of the uncemented sand with water may be very close to that of the cemented sand with gas. Only by understanding the texture of the rock, the interpreter will be able to reliably identify the pore fluid in this situation.

RELATING TEXTURE TO GEOLOGY

A way of identifying rock texture is through comparing the hard velocity and porosity data to geology and depositional features.

It is evident from Figure 7 where the reflection amplitude map is shown at the top of the reservoir that is penetrated by the two wells under examination that Well #2, where the sandstone appears to have slight quartz cementation, is located in the high-energy depositional channel where the sand grains have been stripped of organic coating and grain sorting is good. We speculate that this is one reason for the generation of the contact cement.

On the other hand, Well #1 is located in the low-energy lobe where the large quartz grains are likely to be covered by fines and organics that prevent contact cementation.

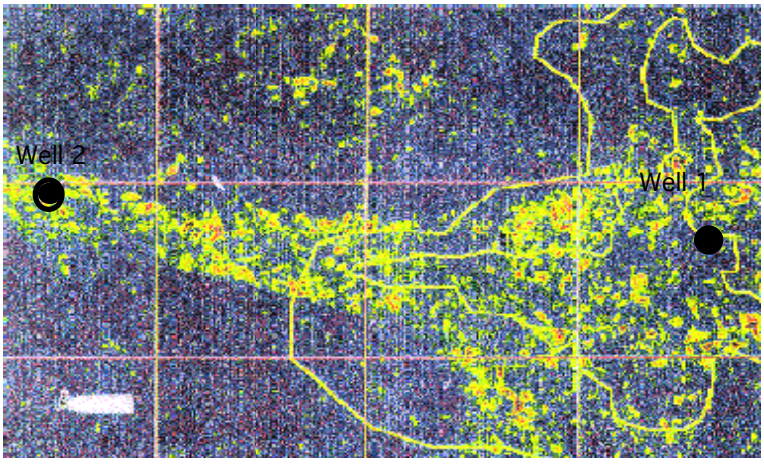

Figure 7. Amplitude map at the top of Heimdal formation with well location.

Therefore, by combining well log and core analysis with the geological knowledge and seismic imaging, we can tell the likelihood of the occurrence of a certain texture (cemented sand in the high-energy environment and friable sand in a lobe).

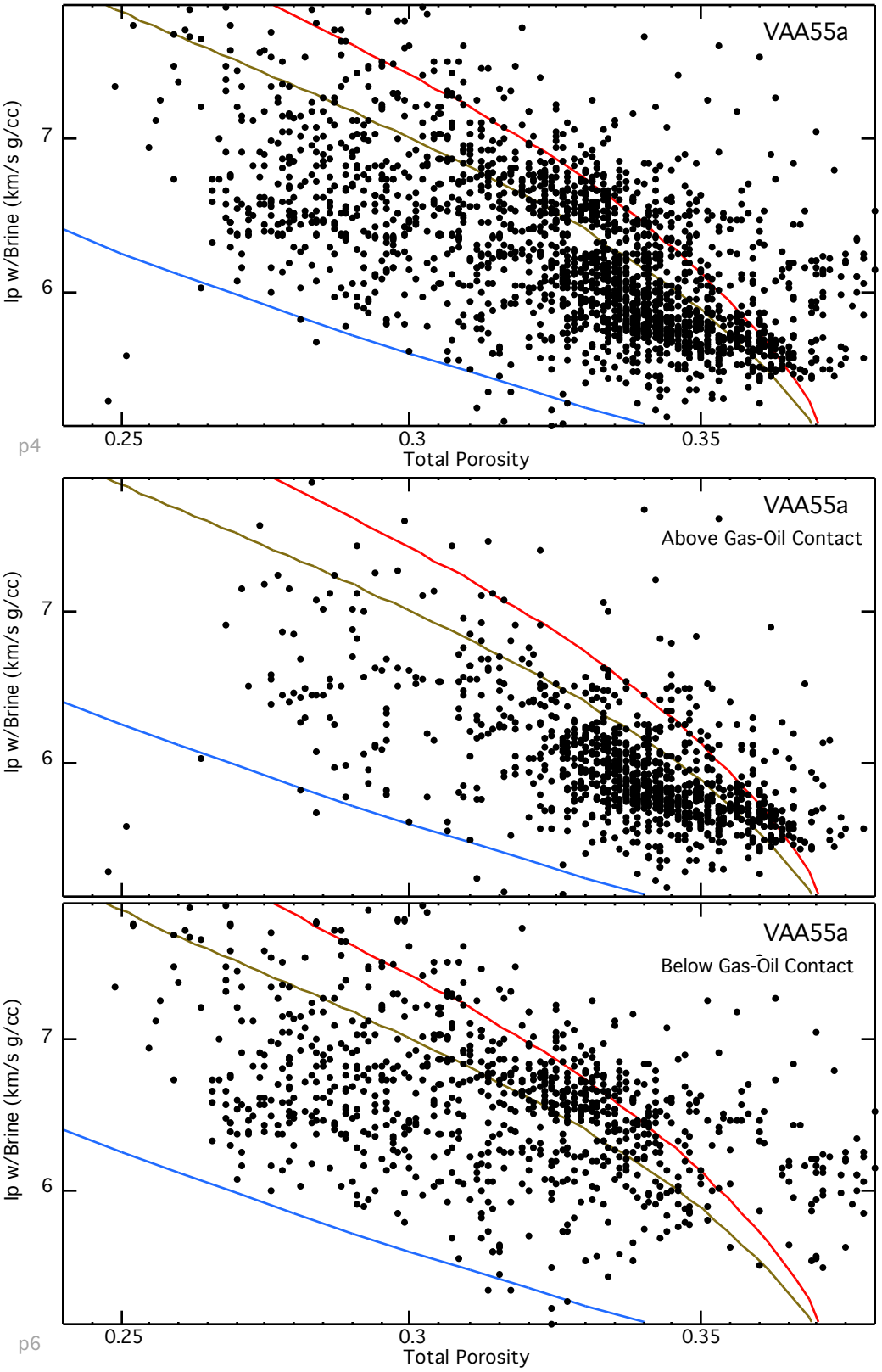
VAA55a
Ip w/Brine (km/s g/cc)
7
6
0.25
0.3
0.35
Total Porosity
p4
VAA55a
Above Gas-Oil Contact
Ip w/Brine (km/s g/cc)
7
6
VAA55a
Below Gas-Oil Contact
Ip w/Brine (km/s g/cc)
7
6
0.25
0.3
0.35
Total Porosity
p6

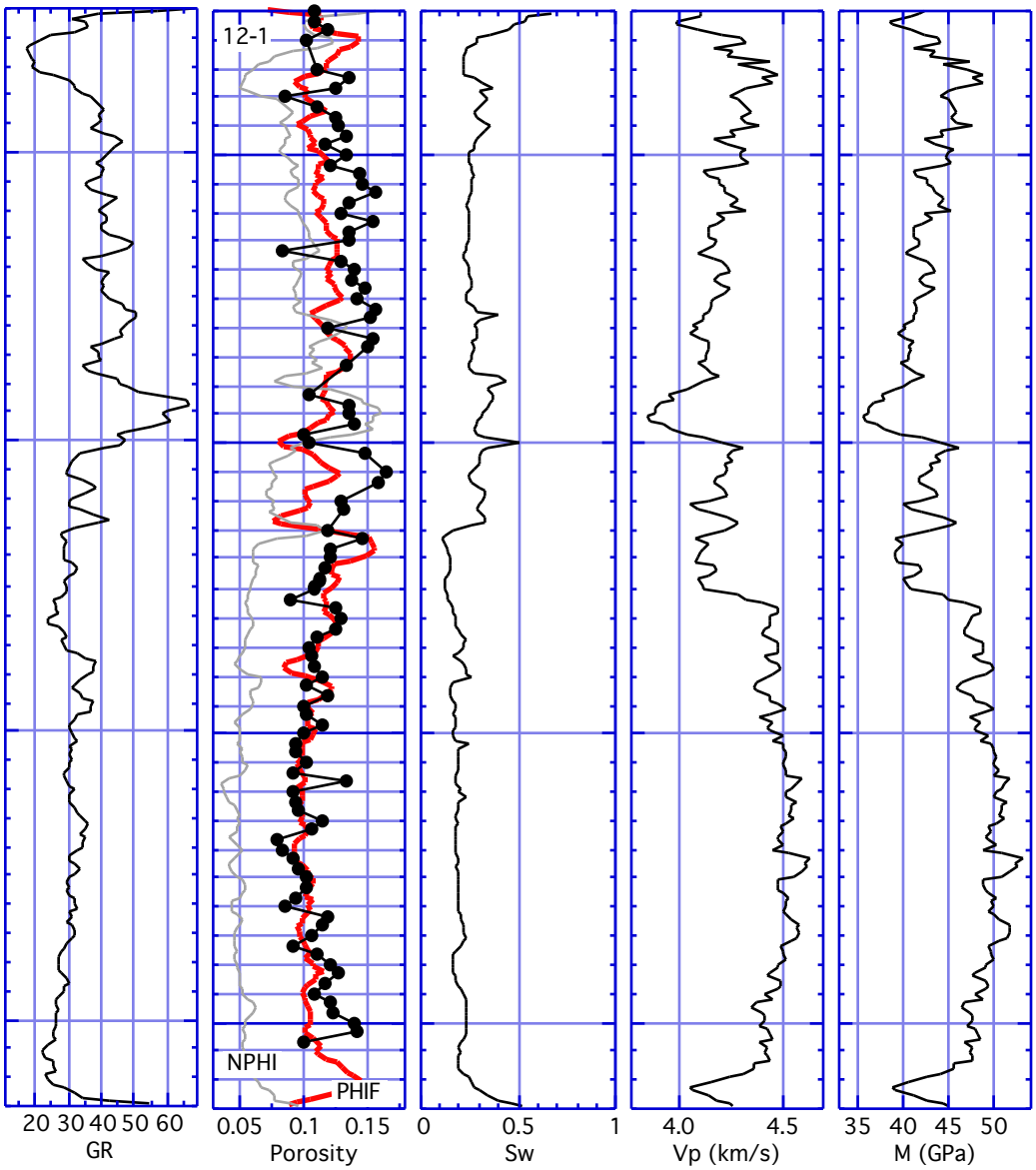
12-1
NPHI
PHIF
20 30 40 50 60
GR
0.05 0.1 0.15
Porosity
0 0.5 1
Sw
4.0 4.5
Vp (km/s)
35 40 45 50
M (GPa)

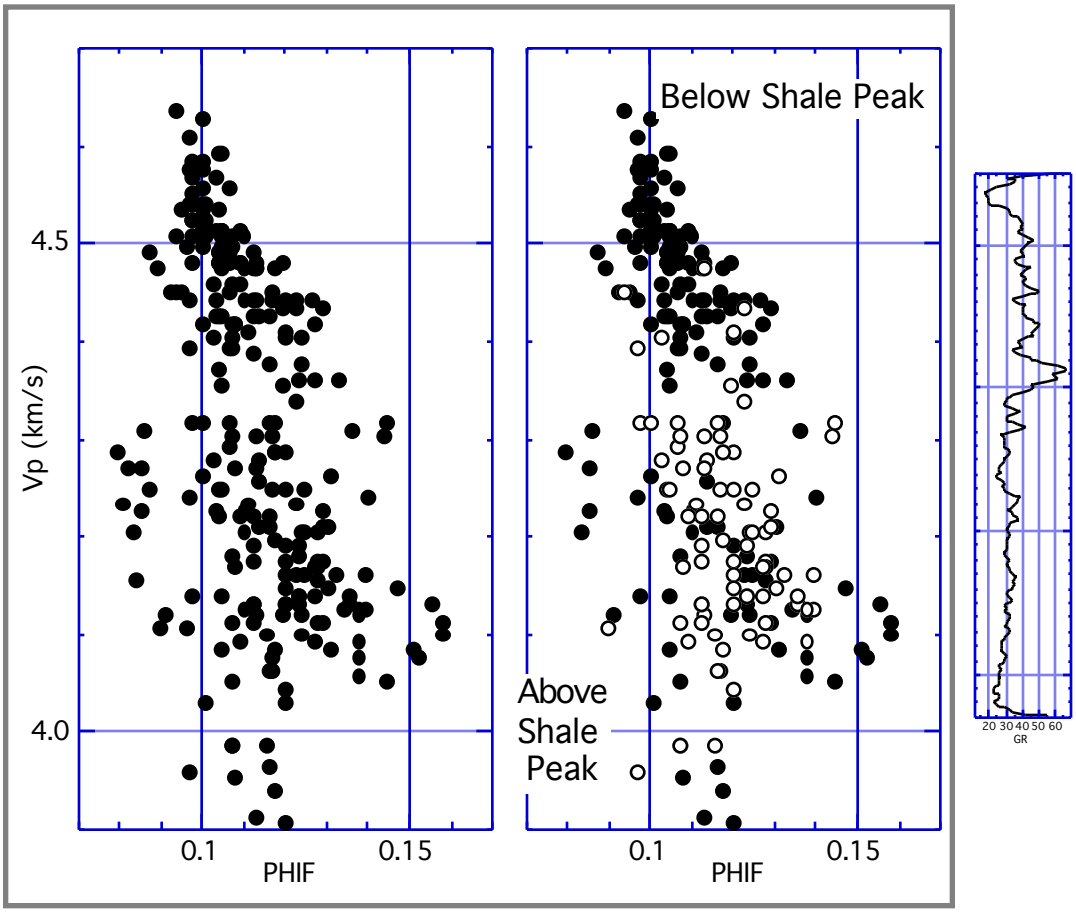
Below Shale Peak
Above
Shale
Peak
Vp (km/s)
4.5
4.0
0.1
0.15
PHIF
0.1
0.15
PHIF
20 30 40 50 60
GR

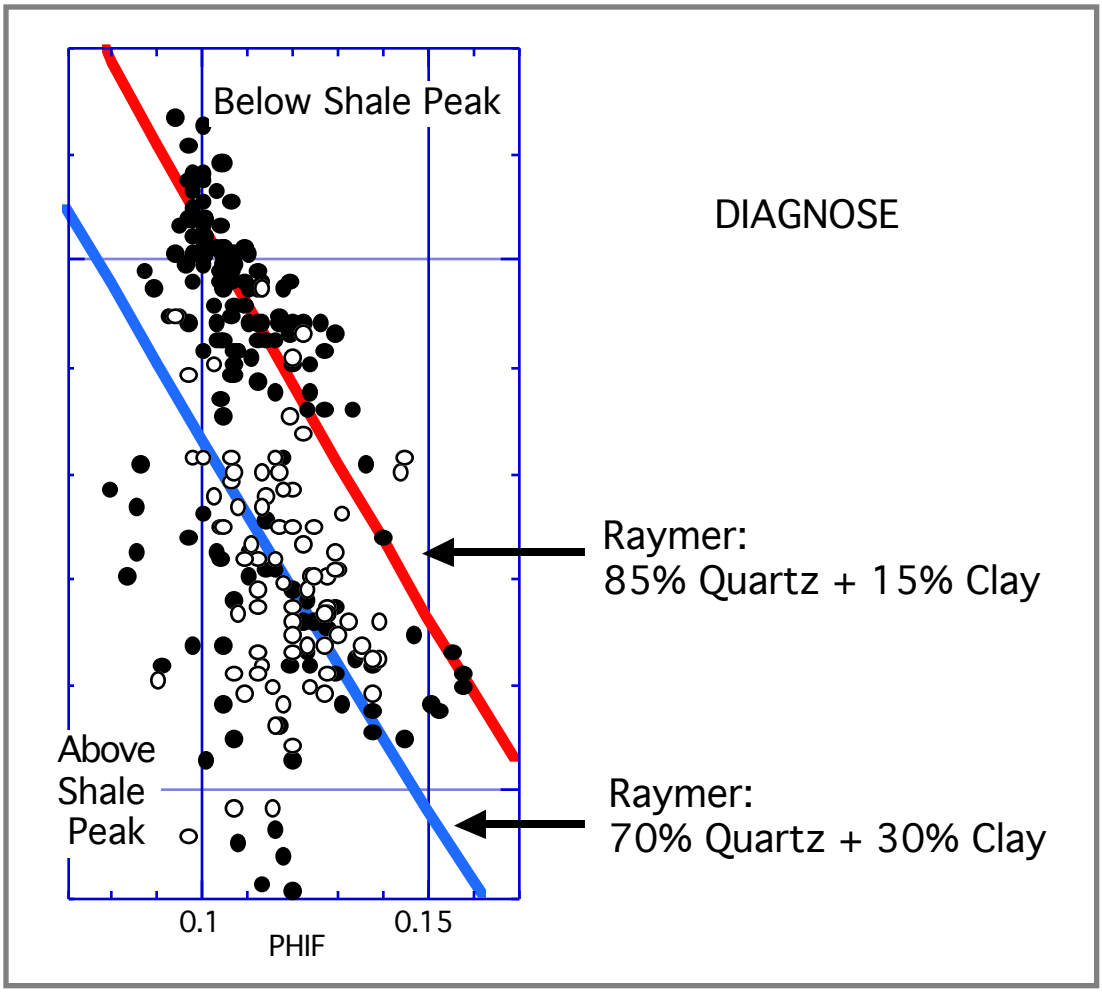
Below Shale Peak
DIAGNOSE
Raymer:
85% Quartz + 15% Clay
Above
Shale
Peak
Raymer:
70% Quartz + 30% Clay
0.1
0.15
PHIF

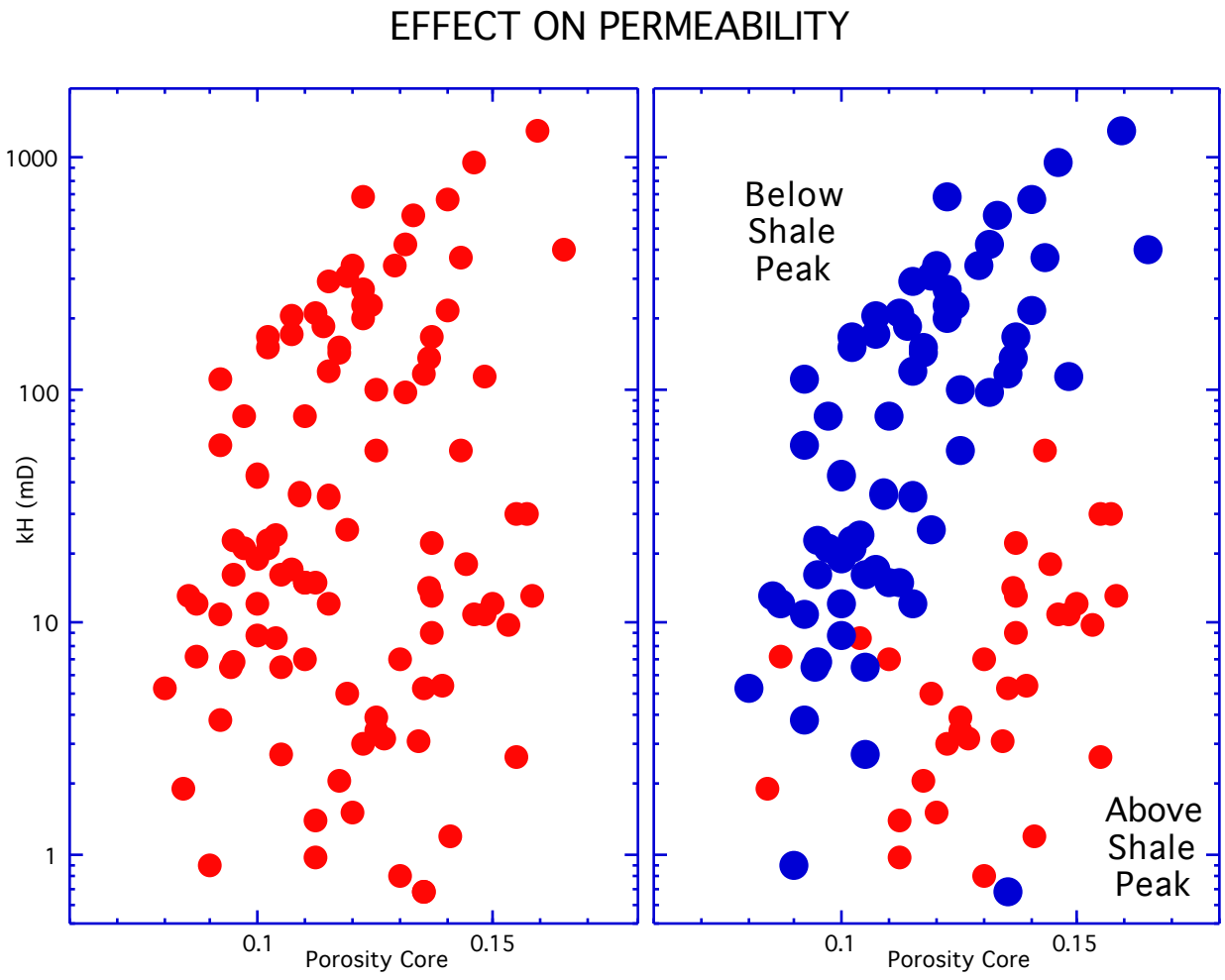
EFFECT ON PERMEABILITY
1000
100
10
1
kH (mD)
0.1
0.15
Porosity Core
Below
Shale
Peak
Above
Shale
Peak
0.1
0.15
Porosity Core